

RECENT DEVELOPMENTS IN SCIENTIFIC RESEARCH III

EDITORS

Prof. Dr. Ayşegül GÜMÜŞ

Assist. Prof. Dr. Gül GÖRMEZ



İKSAD
Publishing House

RECENT DEVELOPMENTS IN SCIENTIFIC RESEARCH III

EDITORS

Prof. Dr. Ayşegül GÜMÜŞ

Assist. Prof. Dr. Gül GÖRMEZ

AUTHORS

Prof. Dr. Ayşegül GÜMÜŞ

Prof. Dr. Evrim ERDEMOĞLU

Prof. Dr. Kemal Kürşat BOZKURT

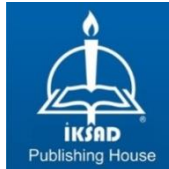
Prof. Dr. Selçuk GÜMÜŞ

Assoc. Prof. Dr. Deniz Türköz ALTUĞ

Assist. Prof. Dr. Gül GÖRMEZ

Assist. Prof. Dr. Ayşegül Feray GÖKDERE

MSc. Serdar TAŞDELEN



Copyright © 2024 by iksad publishing house
All rights reserved. No part of this publication may be reproduced,
distributed or transmitted in any form or by
any means, including photocopying, recording or other electronic or
mechanical methods, without the prior written permission of the publisher,
except in the case of
brief quotations embodied in critical reviews and certain other
noncommercial uses permitted by copyright law. Institution of Economic
Development and Social
Researches Publications®
(The Licence Number of Publisher: 2014/31220)
TÜRKİYE TR: +90 342 606 06 75
USA: +1 631 685 0 853
E mail: iksadyayinevi@gmail.com
www.iksadyayinevi.com

It is responsibility of the author to abide by the publishing ethics rules.
Iksad Publications – 2024©

ISBN: 978-625-378-052-4
Cover Design: İbrahim KAYA
December / 2024
Ankara / Türkiye
Size = 16x24 cm

CONTENTS

PREFACE

Prof. Dr. Ayşegül GÜMÜŞ

Assist. Prof. Dr. Gül GÖRMEZ1

CHAPTER 1

NANOPARTICLE PRODUCTION WITH MEDICINAL PLANTS - HERBAL NANOTECHNOLOGY

Assist. Prof. Dr. Gül GÖRMEZ.....3

CHAPTER 2

PALEOCLIMATIC RECONSTRUCTION WITH PORE WATER CHEMISTRY: AN EXAMPLE FROM LAKE VAN*

Assist. Prof. Dr. Ayşegül Feray GÖKDERE

MSc. Serdar TAŞDELEN.....21

CHAPTER 3

DIAGNOSIS OF HEALTHY AND MALIGNANT HUMAN ENDOMETRIUM TISSUE SAMPLES BY FTIR AND RAMAN SPECTRA

Assoc. Prof. Dr. Deniz Türköz ALTUĞ

Prof. Dr. Kemal Kürşat BOZKURT

Prof. Dr. Evrim ERDEMOĞLU37

CHAPTER 4

SYNTHESIS OF NOVEL FLUORESCENT TRIAZOLE DERIVATIVE AND INVESTIGATION OF ITS ELECTRONIC PROPERTIES

Prof. Dr. Ayşegül GÜMÜŞ

Prof. Dr. Selçuk GÜMÜŞ51

CHAPTER 5

TADF PROPERTIES OF NOVEL D- π -A TYPE OLEDs

Prof. Dr. Selçuk GÜMÜŞ

Prof. Dr. Ayşegül GÜMÜŞ.....69

PREFACE

Scientific advancements over the past century have been remarkable, with significant acceleration over the last 20–30 years. This book aims to showcase ongoing research conducted by various university laboratory groups. It comprises five chapters covering diverse fields such as chemistry, molecular biology, pharmacy, medicine, biotechnology, and physical chemistry.

The first chapter focuses on the production of nanoparticles using medicinal plants.

The second chapter explores paleoclimatic reconstruction through pore water chemistry, using Lake Van as a case study.

In the third chapter, FTIR and Raman spectroscopy are employed to diagnose healthy and malignant human endometrial tissue samples.

The fourth chapter presents findings on the synthesis of a novel fluorescent triazole derivative and the investigation of its electronic properties.

The final chapter delves into the TADF properties of novel D- π -A type OLEDs in depth.

We deeply appreciate the remarkable contributions of all those involved in this publication. Our special thanks go to the İKSAD Publishing family, the scientific committee, the authors, and the readers for their invaluable efforts in the preparation, design, and printing of this book.

Prof. Dr. Ayşegül GÜMÜŞ
Dr. Öğr. Üyesi Gül GÖRMEZ

CHAPTER 1
NANOPARTICLE PRODUCTION WITH MEDICINAL
PLANTS - HERBAL NANOTECHNOLOGY

Assist. Prof. Dr. Gül GÖRMEZ¹

DOI: <https://dx.doi.org/10.5281/zenodo.14503486>

¹ Van Yuzuncu Yil University, Faculty of Health Sciences, Nutrition and Dietetics Department, Van, Türkiye. gulgormez@hotmail.com <https://orcid.org/0000-0001-6980-4988>

INTRODUCTION

Medicinal plants, the primary source of traditional medicine, have been used for thousands of years to protect human health and treat diseases. Plants used as preventive and curative in ancient Egyptian, Indian, Chinese, and Islamic civilizations have formed an essential basis for developing modern medicines. Plants have started to play an important role in contemporary science because of their therapeutic properties and new developments in biotechnology and nanotechnology.

In recent years, active substances such as alkaloids, flavonoids, terpenoids, and polyphenols obtained from medicinal plants have been combined with nanotechnology thanks to their chemical and biological properties, enabling critical environmental, agricultural, and biomedical applications. Plant active ingredients, which form the basis of therapeutic agents used in the treatment of various diseases, are seen as a unique source for nanoparticle production due to their ability to reduce and stabilize metal ions, as well as their environmental compatibility, low cost, and fewer side effects than synthetic drugs. Green synthesized nanoparticles will likely be an effective carrier in drug delivery systems and may offer high bioavailability even at low doses. However, the lack of production efficiency and standardization, the difficulty of large-scale production of green synthesis methods, and the fact that plant extracts contain impurities that may affect the properties of nanoparticles are seen as limiting factors for the use of plant active ingredients in nanoparticle production.

Herbal medicines are gaining global popularity due to their ability to treat, maintain, and enhance health, as well as prevent and address many ailments, as they are perceived to be safer and more cost-effective than traditional pharmaceuticals. Nevertheless, many of these physiologically active phytochemical elements exhibit limits; specifically, their absorption and distribution are suboptimal, and their target selectivity is typically low, leading to diminished bioavailability and reduced biological activity. Moreover, substantial quantities are necessary to elicit the effects of these phytochemical substances, which are also vulnerable to acidic environments and exhibit limited stability (Wang et al., 2014). Nanoparticle production with

medicinal plants has the potential to be sustainable, natural, and future-proof. Green synthesis biological nanoparticle drugs should be subjected to rapid and mass production as fast as synthetic drugs used in modern medicine. In addition, nanoparticle standardization will increase treatment options with more natural products in the future. Therefore, this field needs further research and interdisciplinary cooperation.

1. MEDICINAL PLANTS

Medicinal plants are botanical resources utilized in the prophylaxis and management of ailments. The significance encompasses therapeutic applications as well as cultural and economic elements. These plants are resorted to in light of the indigenous knowledge and practices concerning health nutrition passed down through generations. Thanks to the secondary metabolites they produce, they have been the cornerstone of the traditional medicine system since ancient times. The bioactive compounds (secondary metabolites) may act as a backbone for new pharmaceutical development because many drugs available in the modern pharmacopeia are derived directly or indirectly from plants (Salmerón-Manzano et al., 2020). The use of medicinal plants dates back to the earliest periods of human history. Historical documents from the great civilizations that retook the stage prove the importance of medicinal plants. In archaeological excavations, it has been determined that plants have been used to treat diseases since the Paleolithic Age. In Shennong Materia Medica (2800 BC), one of the oldest medical sources of China, it is reported that plants such as ginseng, ginger, and evening primrose, which are among the essential plants whose effects are still proven today, are widely used in Chinese medicine (Petrovska, 2012). In ancient Egypt, how approximately 650 different plants were used in medicine and for which diseases they were suitable have survived to the present day with the Ebers Papyrus (1550 BC) (Jamshidi-Kia & Lorigooini, 2017). In the medieval Islamic world, mainly Ibn Sina studied medicinal plants in detail and provided detailed information on their pharmacological properties and how to use them (Ackerknecht, 2016). In the Renaissance period, when the foundations of modern chemistry were laid, it became possible to isolate the active components of medicinal plants, which started to be used in treatment (Shakya, 2016). Medicinal plants are essential for human life because of their

therapeutic value, cultural relevance, and economic possibilities. Their integration into the traditional or contemporary health system necessitates more research and preservation to guarantee future availability.

Today, medicinal plants are essential in both traditional medicine and modern biotechnological research. According to the World Health Organization (WHO), 80% of the world's population still uses medicinal plants to meet their basic health needs. Most modern medicines are derived from the secondary metabolites of these plants (Pan et al., 2014).

1.1.Medicinal Plant Active Ingredients Secondary metabolites

Although not directly related to growth, development, or reproduction, plant secondary metabolites are diverse chemical molecules that impact how plants interact with their environment. Secondary metabolites are vital to plant survival because they serve as a defense mechanism and facilitate environmental interactions. Understanding the several elements that control these metabolites would enhance farming methods and encourage the sustainable use of plant resources for commercial and medical applications. According to Khade et al. (2023), these substances fall into several distinct groups, such as phenolic compounds, alkaloids, flavonoids, and terpenoids, each of which has a variety of functions. De et al., 2023).

1.1.1. Terpenoids:

These secondary metabolites are a very diverse group that includes monoterpenes, sesquiterpenes, and diterpenes. They are produced from five-carbon isoprene units. Terpenoids are essential for drawing pollinators and seed dispersers, and they significantly improve a plant's resistance to diseases and herbivores. They also perform crucial roles in the interactions between plants and their environment. These compounds are important in nanoparticle production because of their reduction and stabilization functions. Studies with *Withania somnifera* (Ashwagandha) extract have shown that silver and gold nanoparticles are synthesized efficiently (Tripathi et al.,2019).

1.1.2. Phenolic Compounds:

One or more hydroxyl groups connected to an aromatic ring characterize this large class of molecules. Defensive mechanisms and ecological interactions are among the numerous functions of these compounds, which are abundant in plants. They take a role in protecting plants from herbivores. Additionally, because phenolic chemicals give fruits and flowers color and flavor, they also help draw pollinators. Flavonoids, a subgroup of phenolic compounds, are particularly noted for antioxidant properties and health benefits (Dias et al., 2016). Phenolics and flavonoids prevent oxidation by stabilizing nanoparticles. *Azadirachta indica* (Neem) leaves' phenolics exhibited strong reducing properties in silver nanoparticle synthesis (Chandra et al., 2020).

1.1.3. Alkaloids:

Alkaloids are pharmacologically active and consist of nitrogen atoms. Most plants produce them as a defense mechanism against herbivores and pathogens because they are toxic (Kumar et al., 2023). Some common examples are caffeine and nicotine, which have been studied quite far for medicinal purposes, along with morphine. Environmental stress and biotic stressors can affect alkaloid production, and its production shows natural adaptation (Han et al., 2022). Alkaloids play a decisive role in reducing metal ions to nanoparticles. Extracts of plants such as *Catharantus roseus* have shown the active role of alkaloids in silver nanoparticle synthesis (Mittal et al.).

2. NANOPARTICLE PRODUCTION AND HERBAL NANOPARTICLES

Nanoparticles are particles with dimensions on the nanometer scale, typically ranging between one and a hundred nanometers. Such physical and chemical properties may differ significantly from bulk, making nanoparticles useful in many applications: medicine, electronics, and environmental sciences, among others. Nanotechnology is a key and dynamic domain within contemporary science. Biological, physical, and chemical strategies are followed to synthesize nanoparticles with diverse sizes and forms. Biological

or green synthesis is the most efficient approach for obtaining nanoparticles in an environmentally benign manner, without high pressure, elevated temperatures, excessive energy, or hazardous chemicals (Sinha et al., 2015). Different techniques may be used to synthesize those nanoparticles; the major ones are divided into the following groups: physical, chemical, and biological methods.

Physical methods of nanoparticle production involve the mechanical or thermal processing of materials to create nanoparticles. Techniques like sputtering, ball milling, and laser ablation fall under this category. It is known that these methods provide nanoparticles with uniform size and shape. However, these techniques are less appropriate for large-scale manufacturing because they are frequently costly and energy-intensive. A high-energy laser is used in laser ablation to evaporate a target material, which then cools and condenses into nanoparticles (Yuan & Bomma, 2021).

Chemical Methods for the Production of Nanoparticles involve various chemical synthesis methods to reduce metal salts or other precursors to nanoparticles. Some standard techniques are chemical reduction, sol-gel processes, and co-precipitation. Although several techniques can yield high-quality nanoparticles, they typically utilize hazardous chemicals and solvents, presenting environmental and safety issues (Khandsuren & Prokish, 2021). For example, the chemical reduction of silver nitrate using reducing agents like sodium borohydride can yield silver nanoparticles, but the process may leave behind harmful residues (Adewale et al., 2020).

Nanoparticles can be classified based on composition, shape, and synthesis method. The most common types include:

Metallic Nanoparticles:

This group contains gold (AuNPS), silver (AgNPs), and copper nanoparticles, which have been extensively researched for their catalytic, electrical, and optical characteristics. Metallic nanoparticles are frequently employed in medication delivery systems, sensors, and antibacterial agents (Kapoor et al., 2021).

Metal Oxide Nanoparticles:

This group comprises zinc oxide (ZnO), titanium dioxide (TiO₂), and iron oxide (Fe₂O₃) nanoparticles. Metal oxide nanoparticles are recognized for their photocatalytic characteristics and are utilized in applications including environmental cleanup and UV protection (Shafiee et al., 2021).

Polymeric Nanoparticles

These are composed of polymers and are used for drug delivery and controlled release. They can also be engineered to respond to certain stimuli, such as pH or temperature variations, improving their medicinal efficacy (Hah et al., 2011).

Lipid-Based Nanoparticles:

Liposomes and solid lipid nanoparticles fall under this category. They are used for drug delivery systems, providing a biocompatible and effective means of transporting therapeutic agents (Xu et al., 2022).

Ceramic Nanoparticles

They are typically silica (SiO₂) and calcium phosphate nanoparticles. They are usually used for bone regeneration and drug transportation.

Another nanosynthesis method, green synthesis, better known as biological nanosynthesis, has become an important aspect of nanotechnology due to its environmentally benign, economical, and sustainable nature. It uses natural biological systems such as plant extracts, microorganisms, and enzymes to produce nanoparticles without hazardous chemicals and energy-intensive processes. Its importance lies in enabling the fabrication of biodegradable and functional nanomaterials specifically designed to meet needs in healthcare, agriculture, and environmental cleanup. Biological or green synthesis employs biological organisms, including plants, bacteria, and fungi, to generate nanoparticles. This approach is becoming increasingly popular because of its environmental sustainability and capacity to create nanoparticles without hazardous chemicals. Plant extracts can function as both reducing and stabilizing agents, enabling the one-step production of nanoparticles (Chahardooli & Khodadadi, 2014). Research shows that silver

nanoparticles synthesized using plant extracts exhibit significant antibacterial properties, making them suitable for medical use (Moond et al., 2022).

3. ADVANTAGES AND DISADVANTAGES OF HERBAL NANOPARTICLES

Herbal medicines are gaining global popularity due to their ability to treat, maintain, and enhance health, as well as prevent and address many ailments, as they are perceived to be safer and more cost-effective than traditional pharmaceuticals. Nonetheless, numerous physiologically active phytochemical elements demonstrate limitations; mainly, their absorption and distribution are inadequate, and their target selectivity is generally low, resulting in decreased efficacy and reduced cellular activity. Furthermore, significant amounts are required to produce the effects of these plant-based substances, which are susceptible to acidic conditions and demonstrate low stability. Different approaches to synthesizing herbal nanoparticles have received tremendous attention in the past decade due to their probable advantages and disadvantages in widespread applications, ranging from medicine to pharmaceutical drug delivery systems. Applying plant extracts to produce nanoparticles aims to enhance the bioavailability and activity of herbal compounds.

The most known advantages include the enhanced therapeutic effect, fewer side effects, and stability of herbal formulations. Significant disadvantages include potential toxicity, variation in the synthesis products, and stringency characterization and standardization.

The first significant benefit of the production of herbal nanoparticles is the increase in the bioavailability of active ingredients of medicinal plants. The application of nanoparticles contributes to better absorption in the body of these compounds and improves poorly soluble herbal drugs, at least in absorption rate. Bargude et al. (2023) reported that herbal extracts improve the solubility and stability of nanostructured systems and increase the therapeutic efficacy of the nanoparticle. Moreover, this application of nanotechnology in herbal medicine allows for the targeted delivery of drugs that minimize systemic side effects and lead to better patient compliance (Ambwani et al., 2018). Targeted delivery is important in the treatment of

serious chronic diseases such as cancer and diabetes, where the precise delivery of therapeutic agents is highly crucial (Viswanathan et al., 2018).

Research indicates that nanoparticles derived from diverse plant extracts display notable antibacterial properties, a phenomenon linked to their diminutive size and extensive surface area (Kathik et al., 2018). Nanoparticles derived from *Aloe vera* and *Tridax procumbens* have demonstrated efficacy in inhibiting bacterial growth, indicating their potential applications in textiles and medicine. The capacity of these nanoparticles to infiltrate bacterial cells and interfere with cellular functions highlights their promise as potent antimicrobial agents (Karthik et al., 2020).

Herbal nanoparticles provide therapeutic benefits and improve the stability of herbal formulations. Using natural biopolymers, including chitosan, in nanoparticle synthesis enhances stability and biocompatibility (Kuppusamy et al., 2016; Verma et al., 2021). The stability of herbal medicines is essential for preserving their efficacy throughout storage and application. The green synthesis of nanoparticles utilizing plant extracts represents an environmentally sustainable method that corresponds with the increasing need for biodegradable materials in the pharmaceutical industry (Wang et al., 2016; Kuppusamy et al., 2016).

Despite the benefits, several drawbacks are associated with the production of herbal nanoparticles. The potential toxicity of nanoparticles, stemming from their size, shape, and surface properties, is a primary concern. Numerous studies have indicated the biocompatibility of herbal nanoparticles; however, comprehensive toxicity assessments are necessary to confirm their safety for human application. The variability in the composition of plant extracts can result in inconsistent outcomes in nanoparticle synthesis, thereby impacting their therapeutic efficacy and safety (Islam et al., 2021; Nidianti et al., 2022).

Various factors, including the synthesis process, plant material selection, extraction methods, and synthesis conditions, are important in the characterization and standardization of the properties of plant nanoparticles (Singh et al., 2016). These important factors may cause differences in size, morphology, and surface charge, and thus, the properties of nanoparticles may

change (Gowda et al., 2020; Koliyote & Shaji, 2023). In addition, the necessary approval process for nanoparticle-based plant products and more extensive testing compared to traditional plant products are the difficulties of the sections of nanotechnology in plant medicine (Ambwani et al., 2018).

Production of herbal nanoparticles offers a promising way to increase the therapeutic potential of plant-based directed. Benefits such as improved bioavailability, targeted product, and anti-microbial properties pave the way for using plant nanoparticles in modern medicine. However, challenges such as potential stress, variability, and difficulties in synthesis are being addressed in detail to ensure the safe and effective feeding of herbal nanoparticles. Future research should focus on optimizing synthesis methods, pursuing general potency studies, and developing standard protocols for characterization to fully explore the potential of herbal nanoparticles in therapeutic applications.

4. FUTURE PERSPECTIVES ON HERBAL NANOPARTICLES

Herbal nanoparticles are a new and interesting area of plant-based medicine that could make treatments much more effective. By combining traditional herbal remedies with modern nanotechnology, these nanoparticles make herbal compounds more bioavailable, allowing for more exact targeting and even adding strong antimicrobial properties. Despite that, this field does have some problems. Variability during synthesis, the possibility that stress will affect nanoparticles, and the lack of generally agreed-upon standards are all slowing down progress.

Researchers must enhance synthesis processes to guarantee uniformity in size, shape, and surface characteristics. Standardizing the ways that plant nanoparticles are described will not only help make studies more consistent but also boost faith in science. Moreover, extensive longitudinal investigations on safety and efficacy are essential to satisfy regulatory standards and guarantee that these nanoparticles can safely go from laboratory settings to practical therapeutic applications.

Interdisciplinary collaboration across materials science, biology, and pharmacology may yield the essential breakthroughs to fully realize the

potential of herbal nanoparticles. By tackling these difficulties, we can advance the safety, efficacy, and accessibility of plant-based treatments for various medicinal purposes.

CONCLUSION

The problems with herbal medicines can be fixed by nanotechnology-based transport systems that carry drugs, making phytochemicals more bioavailable and active. The use of nanotechnology is a hopeful new way to improve the curative effects of herbal medicines by making phytochemical components perform better. Many researchers are trying to make a drug delivery method that works well and is safe. New developments in nanotechnology have made people more interested in plant medicines. Using nanotechnology-based delivery methods for phytochemicals is important for public health worldwide. Herbal treatments are being used more and more around the world. However, they are not very well soluble, bioavailable, or effective as drugs because they are not physically or chemically stable and easily broken down. This means that they cannot be used in clinical settings as medicines. Another way to improve the pharmacological effectiveness of herbal medicines could be to combine them with nanotechnology-based delivery methods. Still, these nanotechnology-based delivery methods need more research, especially on their safety and toxicity profiles, to ensure they are safe and effective at treating various illnesses.

REFERENCES

- Ackerknecht, E.H. A Short History of Medicine; Ronald Press: New York, NY, USA, 1955; p. 304. ISBN 978-0801827266.
- Adewale, O. B., Egbeyemi, K. A., Onwuelu, J. O., Potts-Johnson, S. S., Anadozie, S. O., Fadaka, A. O., ... & Onasanya, A. (2020). Biological synthesis of gold and silver nanoparticles using leaf extracts of *Crassocephalum rubens* and their comparative in vitro antioxidant activities. *Heliyon*, 6(11). DOI: 10.1016/j.heliyon.2020.e05413
- Ambwani, S., Tandon, R., Ambwani, T. K., & Malik, Y. S. (2018). Current knowledge of nano delivery systems and their beneficial applications in enhancing the efficacy of herbal drugs. *Journal of Experimental Biology and Agricultural Sciences*, 6(1), 87-107. [https://doi.org/10.18006/2018.6\(1\).87.107](https://doi.org/10.18006/2018.6(1).87.107)
- Bargude, S. D., Chopade, G. L., Pondkule, A. V., Nagrale, S. N., & Babar, V. B. (2023). Nanostructured drug delivery systems: an alternative approach to herbal medicine. *World Journal of Biology Pharmacy and Health Sciences*, 13(1), 099-102. <https://doi.org/10.30574/wjbphs.2023.13.1.0288>
- Chahardooli, M. and Khodadadi, E. (2014). Green synthesis of silver nanoparticles using oak leaf and fruit extracts (*Quercus*) and its antibacterial activity against plant pathogenic bacteria. *International Journal of Biosciences (IJB)*, 97-103. <http://www.innspub.net/wp-content/uploads/2014/02/IJB-V4No3-p97-103.pdf>
- Chandra, H., Kumari, P., Bontempi, E., & Yadav, S. (2020). Medicinal plants: Treasure trove for green synthesis of metallic nanoparticles and their biomedical applications. *Biocatalysis and Agricultural Biotechnology*. <https://doi.org/10.1016/j.bcab.2020.101518>.
- Dias, M. I., Sousa, M. J., Alves, R. C., & Ferreira, I. C. (2016). Exploring plant tissue culture to improve the production of phenolic compounds: A review. *Industrial crops and products*, 82, 9-22. DOI: 10.1016/j.indcrop.2015.12.016
- Dutra, R. C., Campos, M. M., Santos, A. R., & Calixto, J. B. (2016). Medicinal plants in Brazil: Pharmacological studies, drug discovery,

- challenges and perspectives. *Pharmacological Research*, 112, 4-29. DOI: 10.1016/j.phrs.2016.01.021
- Gowda, S. K., M, R. K., Ahmed, S. S., Kowti, R., K, A., & Ramesh, B. (2020). Importance of nanoparticulate systems in emerging biomedical research - an update. *International Journal of Research in Pharmaceutical Sciences*, 11(SPL4), pp. 2134–2140. <https://doi.org/10.26452/ijrps.v11spl4.4433>
- Hah, H. J., Kim, G., Lee, Y. E. K., Orringer, D. A., Sagher, O., Philbert, M. A., & Kopelman, R. (2011). Methylene blue-conjugated hydrogel nanoparticles and tumor-cell targeted photodynamic therapy. *Macromolecular bioscience*, 11(1), 90-99. DOI: 10.1002/mabi.201000271
- Han, D., Wang, K., Long, F., Zhang, W., Yao, X., & Chen, S. (2022). Effects of endophytic fungi on the secondary metabolites of *Hordeum bogdani* under alkaline stress. *AMB Express*, 12(1), 73. DOI: 10.1186/s13568-022-01388-0
- Islam, R., Sun, L., & Zhang, L. (2021). Biomedical applications of Chinese herb-synthesized silver nanoparticles by phytonanotechnology. *Nanomaterials*, 11(10), 2757. <https://doi.org/10.3390/nano11102757>
- Jamshidi-Kia, F., Lorigooini, Z., & Amini-Khoei, H. (2017). Medicinal plants: Past history and future perspective. *Journal of herbmed pharmacology*, 7(1), 1–7. DOI: 10.15171/jhp.2018.01
- Kapoor, R. T., Salvadori, M. R., Rafatullah, M., Siddiqui, M. R., Khan, M. A., & Alshareef, S. A. (2021). Exploration of microbial factories for synthesis of nanoparticles—a sustainable approach for bioremediation of environmental contaminants. *Frontiers in Microbiology*, p. 12, 658294.
- Karthik, S., Saha, R., Palanisamy, S., Shanmugam, B. K., Rangaraj, S., Murugan, V. S., ... & Aicher, W. K. (2020). Wet chemical preparation of herbal nanocomposites from medicinal plant leaves for enhanced coating on textile fabrics with multifunctional properties. *SN Applied Sciences*, 2(4). <https://doi.org/10.1007/s42452-020-2459-z>
- Karthik, S., Shanmugam, B. K., Rangaraj, S., Manivasakan, P., Periasamy, P., & Rajendran, V. (2018). Screening the UV-blocking and

- antimicrobial properties of herbal nanoparticles prepared from aloe vera leaves for textile applications. *IET Nanobiotechnology*, 12(4), 459–465. <https://doi.org/10.1049/iet-nbt.2017.0097>
- Khade, O. S., Sruthi, K., Sonkar, R. M., Gade, P. S., & Bhatt, P. (2023). Plant secondary metabolites: extraction, screening, analysis and their bioactivity. *International Journal of Herbal Medicine*, 11(2), 01-17. DOI: <https://doi.org/10.22271/flora.2023.v11.i2a.855>
- Khandsuren, B., & Prokisch, J. (2021). The production methods of selenium nanoparticles. *Acta Universitatis Sapientiae, Alimentaria*, 14(1), 14-43. DOI: 10.2478/ausal-2021-0002
- Koliyote, S. and Shaji, J. (2023). A recent review on synthesis, characterization, and activities of gold nanoparticles using plant extracts. *Indian Journal of Pharmaceutical Education and Research*, 57(2s), s198-s212. <https://doi.org/10.5530/ijper.57.2s.24>
- Kuppusamy, P., Yusoff, M. M., Maniam, G. P., & Nagarajan, G. (2016). Biosynthesis of metallic nanoparticles using plant derivatives and their new avenues in pharmacological applications – an updated report. *Saudi Pharmaceutical Journal*, 24(4), 473-484. <https://doi.org/10.1016/j.jsps.2014.11.013>
- Mittal, A., Chisti, Y., & Banerjee, U. (2013). Synthesis of metallic nanoparticles using plant extracts. *Biotechnology advances*, p. 31 2, 346–56. <https://doi.org/10.1016/j.biotechadv.2013.01.003>.
- Moond, M., Singh, S., Sangwan, S., Devi, R., & Beniwal, R. (2022). Green synthesis and applications of silver nanoparticles: a systematic review. *AATCC Journal of Research*, 9(6), 272–285. DOI: 10.1080/23308249.2022.2073450
- Nidianti, E., Amalia, R., & Firdaus, N. S. (2022). Toxicity of cisplatin and herbal medicine complexed with bovine serum albumin (BSA) and folic acid nanoparticles as anticancer candidates. *Jurnal Farmasi Galenika (Galenika Journal of Pharmacy) (E-Journal)*, 8(2), 88-96. <https://doi.org/10.22487/j24428744.2022.v8.i2.15838>
- Pan, S. Y., Litscher, G., Gao, S. H., Zhou, S. F., Yu, Z., Chen, H. Q., ... & Ko, K. M. Historical perspective of traditional indigenous medical practices. DOI: 10.1155/2014/495635

- Petrovska, B. B. (2012). Historical review of medicinal plants' usage. *Pharmacognosy reviews*, 6(11), 1. DOI: 10.4103/0973-7847.95849
- Salmerón-Manzano, E., Garrido-Cardenas, J. A., & Manzano-Agugliaro, F. (2020). Worldwide research trends on medicinal plants. *International journal of environmental research and public health*, 17(10), 3376. DOI: 10.3390/ijerph17103376.
- Shafiee, P., Nafchi, M. R., Eskandarinezhad, S., Mahmoudi, S., & Ahmadi, E. (2021). Sol-gel zinc oxide nanoparticles: advances in synthesis and applications. *Synthesis and Sintering*, 1(4), 242-254. DOI: 10.53063/synsint.2021.1424
- Shakya, A. K. (2016). Medicinal plants: Future source of new drugs. *International journal of herbal medicine*, 4(4), 59-64.
- Singh, P., Singh, H., Ahn, S., Castro-Aceituno, V., Pérez, Z. E. J., Simu, S. Y., ... & Yang, D. C. (2016). Pharmacological importance, characterization, and applications of gold and silver nanoparticles synthesized by Panax ginseng fresh leaves. *Artificial Cells, Nanomedicine, and Biotechnology*, 45(7), 1415-1424. <https://doi.org/10.1080/21691401.2016.1243547>
- Sinha SN, Paul D, Halder N, Sengupta D, Patra SK. Green synthesis of silver nanoparticles using the freshwater green alga *Pithophora oogonia* (Mont.) Wittrock and evaluation of their antibacterial activity. *Appl Nanosci* 2015; 5(6): 703-709. DOI: 10.1007/s13204-014-0364-7
- Tripathi, D., Modi, A., Narayan, G., & Rai, S. (2019). Green and cost-effective synthesis of silver nanoparticles from endangered medicinal plant *Withania coagulants* and their potential biomedical properties. *Materials science & engineering. C, Materials for biological applications*, 100, 152–164. <https://doi.org/10.1016/j.msec.2019.02.113>.
- Verma, D. K., Malik, R., Meena, J., & Rameshwari, R. (2021). Synthesis, characterization, and applications of chitosan-based metallic nanoparticles: a review. *Journal of Applied and Natural Science*, 13(2), 544–551. <https://doi.org/10.31018/jans.v13i2.2635>
- Viswanathan, B., Meeran, I., Subramani, A., Ali, J., & Shabeer, T. (2018). Historical review on modern herbal nano gel formulation and delivery

- methods. *International Journal of Pharmacy and Pharmaceutical Sciences*, 10(10), 1. <https://doi.org/10.22159/ijpps.2018v10i10.23071>
- Wang, D., Markus, J., Wang, C., Kim, Y., Mathiyalagan, R., Castro-Aceituno, V., ... & Yang, D. C. (2016). Green synthesis of gold and silver nanoparticles using aqueous extract of cibotium barometz root. *Artificial Cells, Nanomedicine, and Biotechnology*, 45(8), 1548-1555. <https://doi.org/10.1080/21691401.2016.1260580>
- Wang, S., Su, R., Nie, S., Sun, M., Zhang, J., Wu, D., & Moustaid-Moussa, N. (2014). Application of nanotechnology in improving bioavailability and bioactivity of diet-derived phytochemicals. *The Journal of Nutritional Biochemistry*, 25(4), 363–376. DOI: 10.1016/j.jnutbio.2013.12.009
- Xu, L., Wang, X., Liu, Y., Yang, G., Falconer, R. J., & Zhao, C. X. (2022). Lipid nanoparticles for drug delivery. *Advanced NanoBiomed Research*, 2(2), 2100109. DOI: 10.1002/anbr.202100109
- Yuan, Q., Bomma, M., & Xiao, Z. (2021). Enhanced extracellular synthesis of gold nanoparticles by soluble extracts from *Escherichia coli* transformed with *Rhizobium tropici* phytochelatase gene. *Metals*, 11(3), 472. <https://doi.org/10.3390/met11030472>

CHAPTER 2

**PALEOCLIMATIC RECONSTRUCTION WITH PORE WATER
CHEMISTRY: AN EXAMPLE FROM LAKE VAN***

Assist. Prof. Dr Ayşegül Feray GÖKDERE¹

MSc. Serdar TAŞDELEN²

DOI: <https://dx.doi.org/10.5281/zenodo.14503495>

¹ Van Yuzuncu Yil University, Faculty of Engineering, Geological Engineering Department, Van, Türkiye. feraygokdere@yyu.edu.tr <https://orcid.org/0000-0002-3842-1711>

² Van Yuzuncu Yil University, Institute of Nature and Applied Science, Van, Türkiye, geosertasdelen@gmail.com <https://orcid.org/0009-0009-7542-8507>

*This study is partly derived from the MSc thesis titled “The Origin of the Pore Water of the Mud Volcano in the Lake Van Northern Basin” and supported by the Van YYU Scientific Research Projects Coordination Office with the project number 2015-FBE-YL215.

INTRODUCTION

The term pore water is used to describe water trapped within sedimentary rocks or sediments. The composition of this water consists of dissolved ions, organic matter, and isotopes. Pore water chemistry plays a significant role in the comprehension of geochemical processes. The composition and concentration of dissolved substances within the sediment are indicative of biological, physical, and chemical processes occurring within the sedimentary environment. The pore water present in lake sediments provides a unique and invaluable archive for the reconstruction of palaeoenvironmental conditions and climatic changes. This is due to the fact that the characteristics of the waters at the time of deposition are reflected in the pore water, which, therefore, serves as a direct and accurate record of past environmental conditions. The phenomenon of climate change gives rise to a multiplicity of impacts that serve to alter the functioning of ecosystems, water resources, and geochemical cycles on a global scale. Pore water chemistry represents a valuable tool for understanding the long-term effects of changes. For example, changes in precipitation and temperature directly affect the ionic composition and density of the pore water. However, changes in sea and lake water levels also have an impact on the salinity and ionic composition of pore water. Consequently, pore water is used in palaeoclimatic studies as it records the effects of climate change and allows us to establish the relationship between past and present. The present study analyses the chemical properties of pore water and their implications for climate. The chemistry of pore water obtained from a short sediment core taken from Lake Van (Eastern Anatolia/Turkey) was analyzed as a case study, with the aim of examining the relationship between climate change. This study will demonstrate how understanding pore water chemistry can contribute to the analysis of climate change processes. In this context, this book chapter aims to provide new perspectives for research in paleoclimatology and environmental chemistry.

1. THE FUNDAMENTALS OF PORE WATER CHEMISTRY

The primary constituents of pore water, including major ions, trace elements, organic matter, and gases, offer valuable insights into environmental conditions, geochemical processes, and biological activity.

Major ions are used to describe a group of ions that consists of cations and anions. Cations are defined as ions with a positive charge. The major ions present in pore water are sodium (Na^+), potassium (K^+), magnesium (Mg^{+2}), and calcium (Ca^{+2}). Anions are chloride (Cl^-), sulphate (SO_4^-) and carbonate/bicarbonate ($\text{CO}_3^{-2}/\text{HCO}_3^-$). The behavior of these ions is subject to a number of processes, including mineral dissolution, precipitation and iron exchange. For example, the dissolution of gypsum in contaminated lake sediments has been observed to increase the concentration of sulfate ions, thereby altering the major ion composition of pore waters and affecting mineral stability (Rao et al., 2020). In the context of early diagenetic changes, the distribution of major ions in sediment pore water has been demonstrated to be closely linked to sediment compaction and organic matter transformation (Poletaeva et al., 2021).

The presence of trace elements, including $\text{Fe}^{+2}/\text{Fe}^{+3}$, Mn^{+2} , Si, and Al, in pore water serves as a critical indicator of redox conditions and sediment mineralogy. These ions are the result of various biogeochemical processes and reflect prevailing environmental conditions within the sediment. Iron, (Fe^{+2} , Fe^{+3}) plays a significant role in sedimentary redox processes. It has been observed that dissolved iron concentrations can exhibit notable gradients around the sediment-water interface, influenced by factors such as organic matter inputs and sediment dynamics (Zhu & Aller, 2012). This indicates that Fe^{+2} concentrations can provide insight into the redox state of the sediment, with higher concentrations typically more reducing conditions. It is clear from the studies that another component, the concentration of Mn^{+2} in pore water, varies burial depth. This has a direct effect on the geochemical environment and the stability of minerals (Fan et al., 2024).

The decomposition of plant and animal materials (dissolved organic carbon, organic acids, and metabolic by-products of microorganisms), which is the primary source of organic matter, has a considerable impact on the chemical composition of pore water and the overall sediment environment. These components serve as important indicators of biochemical processes and organic matter decomposition, providing insight into the chemical and biological interactions occurring within the system. Haraguchi (2012)

reported that the concentration of phosphorus in pore water is closely related to the content of organic matter. It was observed that higher levels of organic matter generally lead to a greater release of phosphorus. This relationship emphasizes the importance of organic matter in nutrient cycling and its potential impact on eutrophication processes in aquatic systems.

The chemistry of pore water is significantly influenced by gases such as methane (CH_4), carbon dioxide (CO_2) and oxygen (O_2). The concentrations of these gases can provide insights into redox conditions of the sediment, the decomposition of organic matter, and microbial activity. Methane is typically produced in anoxic conditions through microbial processes, and its concentration can serve as an indicator of the extent of anaerobic decomposition of organic matter. In a subtropical freshwater reservoir, sediment pore water was observed to exceed the saturation point for methane concentration, underscoring the pivotal role of sediments as significant methane sources to the atmosphere (Sturm et al., 2014). Noble gases, including helium, neon, and argon, are also present in sediment pore water and can be used as tracers to gain insight into gas dynamics and sedimentary processes. Brennwald et al. (2011) demonstrated that the analysis of dissolved noble gases in pore water can provide information on the transport of gases within sediments and potential external inputs.

2. CLIMATE CHANGE AND PORE WATER CHEMISTRY

The relationship between climate change and pore water chemistry is a crucial area of study for understanding the environmental impacts of climate changes. The chemical constituents of pore water contain residual evidence of past climatic events, which can be used to reconstruct how these events were shaped by a range of factors, including temperature, precipitation patterns and changes in sea/lake level.

An increase in temperature affects pore water chemistry in a number of ways. Elevated temperatures can result in alterations to the ionic composition of pore water, due to the influence of temperature on the solubility of carbonate and silica minerals. To illustrate, the pore water chemistry of the Bratsk reservoir has been shown to be influenced by the high

calcium carbonate content of the sediments. This, in conjunction with temperature variations, can result in notable alterations to the ionic balance, particularly regarding bicarbonate and calcium ions (Poletaeva et al., 2021). The rate of chemical reactions is also affected by climate change. An increase in temperature results in an acceleration of redox reactions and the decomposition of organic matter. These results in an increase in concentrations of dissolved gases, particularly methane (CH₄) and carbon dioxide (CO₂). For example, research has demonstrated that higher temperatures can result in elevated rates of methanogenesis in peatlands and other anaerobic ecosystems, given that microbial activity is often temperature-sensitive (Chuvilin et al., 2022). This is particularly significant in permafrost regions, where the thawing of previously frozen ground due to climate change can result in the release of organic matter that has been trapped there for an extended period. This, in turn, can lead to methane production (Chuvilin et al., 2022). The increased mobility of pore fluids at higher temperatures can facilitate the transport of methane through the sediment, potentially leading to enhanced oxidation processes in overlying water layers (Harrison et al., 2017). The oxygen and hydrogen isotope ratios in pore water are subject to alteration with an increase in temperature. An increase in temperature accelerates the rate of evaporation, which preferentially removes lighter isotopes of water from the liquid phase, thereby enriching the remaining water in heavier isotopes (Beria et al., 2018). This process can result in notable alterations to $\delta^{18}\text{O}$ and $\delta^{16}\text{D}$ values of pore water, particularly in shallow aquifers and wetlands where evaporation rates are elevated (Mattei et al., 2020). The use of isotopic data in palaeotemperature estimates is a common practice. Temperature-dependent isotopic equilibrium conditions can be determined using the method defined for measuring stable isotopes in pore water (Koehler et al., 2020).

Changes in precipitation regime exert a direct influence on pore water chemistry. Increased precipitation may result in a reduction in ion concentrations due to the dilution effect of pore water. The correlation between precipitation and source water can impact the Ca/Mg and other ionic compositions in pore water. The precipitation regime can accelerate diffusion processes between surface water and pore water, leading to alterations in the

chemical balance of pore water. A study conducted in saline environments demonstrated that the influx of precipitation reduces the salinity of pore water, thereby influencing the availability of nutrients and overall biogeochemical processes occurring within the sediment (Khosravi et al., 2018).

The fluctuation of sea level has a significant impact on the chemical composition of pore water in coastal and marine sediments. An increase in sea level can result in saltwater intrusion into sediments, increasing Cl and Na concentrations. A reduction in salt concentration is observed in the context of sea level decline. The interaction of brine with pore water can alter the chemistry of the water, resulting in the dissolution of evaporite minerals such as halite. Salinity fluctuations impact the solubility of trace elements, including Ba and Sr, which in turn influence trace element composition of the pore water. One of the most negative consequences of rising sea levels is the increased risk of saltwater intrusion into coastal aquifers. As sea levels rise, the balance between freshwater and saltwater is disturbed, causing saltwater to enter aquifers previously dominated by freshwater. This phenomenon has been documented, which highlights how sea-level rise can exacerbate saltwater intrusion and thus alter the chemical balance of pore water (Rasmussen et al., 2013).

3. PORE WATER CHEMISTRY IN LAKE VAN SEDIMENTS

Lake Van is the largest lake in Turkey and the fourth largest lake in the world in terms of volume (607 km³), area (3750 km²) and depth (451 m). It is also the world's largest soda lake (Degens & Kurtzman, 1978; Litt et al., 2009; Çukur et al., 2015). Lake Van provides an excellent case study for paleoclimatological, palaeoenvironmental, and palaeotectonic research due to its extensive continental history, encompassing both glacial and interglacial periods (Litt et al., 2009). In this context, Lake Van was the subject of an international project, ICDP (International et al.), in 2010. The majority of previous studies have concentrated on palaeoclimatic and palaeoenvironmental characteristics of Lake Van (Landman et al., 1996a, 1996b; Lemcke, 1996; Wick et al., 2003; Litt et al., 2009; Litt et al., 2014; Stoeckle et al., 2012; Stoeckle et al., 2014; Çukur et al., 2012; Çukur et al., 2014; Çağatay et al., 2014; Pickarski et al., 2015; Pickarski et al., 2017). The

statistical models obtained with instrumental data demonstrated that temperature and wind speed are the primary parameters influencing the fluctuations in the water level of Lake Van (Meydan et al., 2022). The precipitation effect was found to be minimal due to the specific characteristics of precipitation in the region, namely snowfall (Meydan et al., 2022). Also, the long-term pore water study observed strong changes in the vertical salinity profiles of pore water, and it was reported that the salinity balance of the lake was almost constant, suggesting that these salinity changes indicate large level changes in the past (Tomonaga et al., 2017). In this context, the objective of this section is to provide insights into the chemistry of pore water within the sediments of Lake Van and to relate it to past climatic variations. In order to achieve this, a short sediment core (Van16-03, 70cm length) was taken from Lake Van (Figure 1).

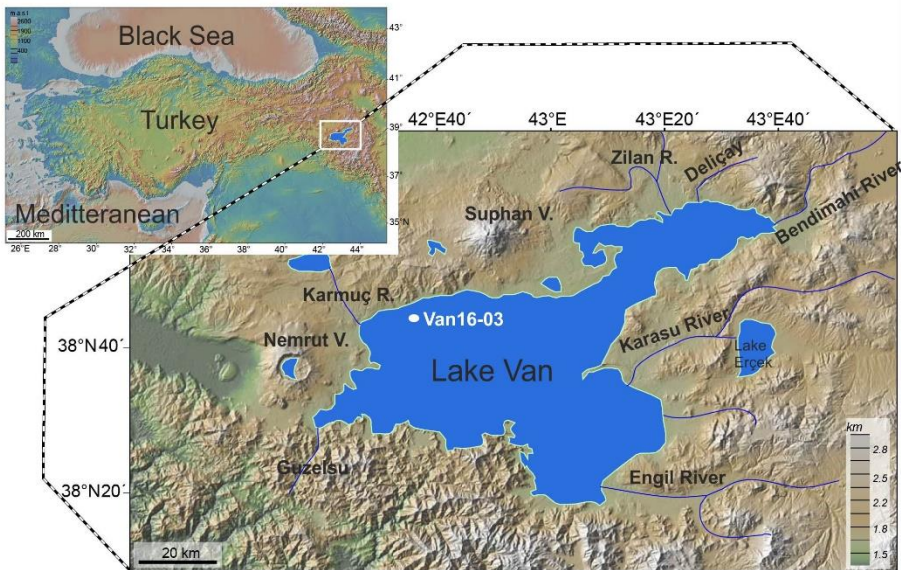


Figure 1. Study area and short core (Van16-03) location (modified from Çukur et al., 2013).

Pore water sampling is based on the principle that samples are taken as efficiently as possible and sent for analysis after being supplemented with chemicals to ensure that the sediment is not disturbed. In order to avoid damaging the structure of the cores, the plastic liners were previously drilled

at 5 cm intervals, and the drilled points were taped to prevent loss of sediments. Subsequently, pore water was sampled in the laboratory using the rhizon sampler (Figure 2). Rhizon samplers comprise a syringe and a porous apparatus (0.15 μm) at the tip of the syringe. The water drawn with the syringe is filtered in the porous apparatus, enabling the acquisition of pore water suitable for analysis without any ion exchange.



Figure 2. Pore water extraction with Rhizon samplers.

Anion analysis by ion chromatography and cation analysis by ICP-MS were performed on the pore waters. The anion-cation values indicate that the order of cations in the water samples is $\text{Na} > \text{K} > \text{Mg} > \text{Ca}$ at all levels. However, the order of anions is $\text{HCO}_3 > \text{Cl} > \text{SO}_4 > \text{CO}_3$ at 15 and 35 cm intervals and $\text{Cl} > \text{HCO}_3 > \text{CO}_3 > \text{SO}_4$ at all other levels. The chemical analysis results obtained from the pore water samples taken from sediment core Van16-03 were transferred to the Piper diagram (Figure 3).

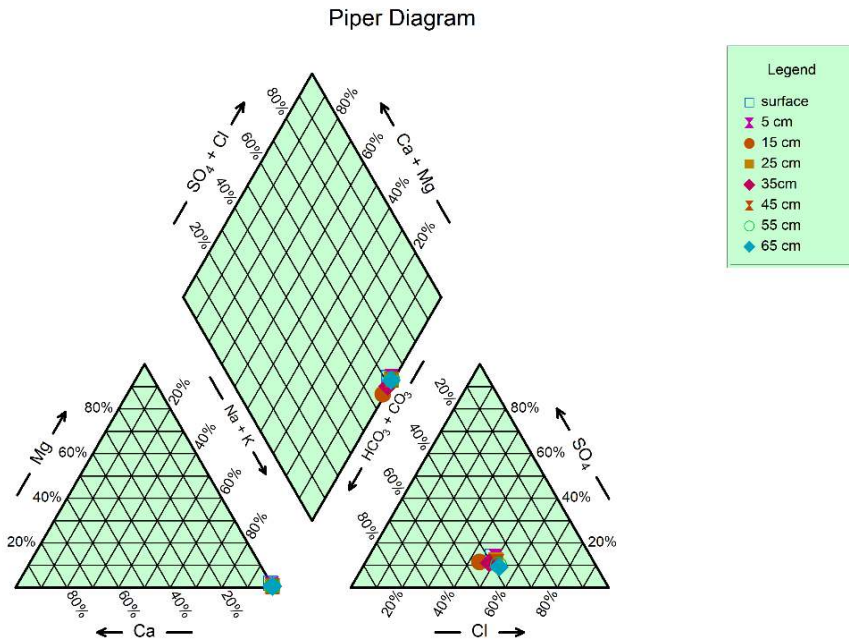


Figure 3. The Piper diagram represents pf pore water according to their chemical properties

Since the short core was taken from a previously dated point, the age was calculated according to depth. The water types according to age are given below (Table 1).

Table 1. Water types according to calender year.

Pore Water	Water Type	Calender Year (AD)
Surface	Na-Cl	2016
5 cm	Na-Cl	1971
15 cm	Na-HCO ₃	1885
25 cm	Na-Cl	1789
35 cm	Na-HCO ₃	1698
45 cm	Na-Cl	1607
55 cm	Na-Cl	1516
65 cm	Na-Cl	1426

It can be posited that over the last 600 years, there has been a shift in the dominant water type, with a Na-HCO₃ water type observed in 1885 AD and 1698 AD and a Na-Cl water type present at all other levels. It is possible to associate these changes with past climate changes. The phenomenon known as the Little Ice Age occurred in the Northern Hemisphere between the 15th century and the 19th century. It is characterized by a cold and dry period (Mann, 2003). The chemical composition of the pore water indicates that the water type is consistent with arid climatic conditions during the LIA. The occurrence of freshwater input suggests a shift in humidity within the basin during the LIA, which in turn implies a change in the precipitation regime and a corresponding influx of freshwater into the lake. This aligns with the observed transition from extreme cold and dry periods to periods of reduced drought intensity during the LIA.

9. CONCLUSION

Pore water chemistry is a significant factor in the study of past climate change. This chapter examines the impact of climatic variables, including temperature increase, fluctuations in precipitation, and sea level, on the composition of pore water. Pore water chemistry is a critical tool for the reconstruction of palaeoclimate data and the understanding of geochemical processes within the sediment. Lake Van pore water study illustrated the capacity to correlate the chemical profiles of pore water with palaeoclimatic events. However, studies of pore water are predominantly limited to data at the regional scale, which presents a challenge for large-scale comparisons. Moreover, the temporal resolution of chemical processes may vary depending on factors such as sediment accumulation rates, which introduces some degree of uncertainty. Notwithstanding these constraints, pore water analysis represents a valuable approach for advancing our understanding of future research. In future studies, integrating pore water chemistry with modern climate models will facilitate a broader climatic context extending from the past to the present. In particular, the combination of isotopic studies and advanced analytical techniques will facilitate a deeper understanding of this field. Furthermore, multidisciplinary approaches may enable a more comprehensive insight into the relationship between pore water chemistry and ecosystem dynamics and environmental processes. In conclusion, as seen şn

the case of Lake Van, pore water chemistry has the potential to provide unique insights into past climate dynamics. This valuable information on past climate changes will inform the development of predictive models for future climate change scenarios and the formation of sustainable environmental management policies.

REFERENCES

- Beria, H., Larsen, J., Ceperley, N., Michelon, A., Vennemann, T., Schaepli, B. (2018). Understanding snow hydrological processes through the lens of stable water isotopes. *WIREs Water*, 5(6). <https://doi.org/10.1002/wat2.1311>
- Brennwald, M. S., Hofer, M., Peeters, F., Hertig, W. A., Strassmann, K., Kipfer, R., Imboden, D. I. (2011). Analysis of dissolved noble gases in the pore water of lacustrine sediments. *Limnology and Oceanography: Methods*, 1, 51-62. doi:10.4319/lom.2011.1.51
- Chuvilin, E., Sokolova, N. A., & Bukhanov, B. (2022). Changes in unfrozen water contents in warming permafrost soils. *Geosciences*, 12(6), 253. <https://doi.org/10.3390/geosciences12060253>
- Cukur, D., Krastel, S., Çağatay, M. N., Damcı, E., Meydan, A. F., Kim, S. (2015). Evidence of extensive carbonate mounds and sublacustrine channels in shallow waters of lake van, eastern Turkey, based on high-resolution chirp subbottom profiler and multibeam echosounder data. *Geo-Marine Letters*, 35(5), 329-340. doi:10.1007/s00367-015-0410-x
- Cukur, D., Krastel, S., Demirel-Schlüter, F., Demirbağ, E., Imren, C., Toker, M. (2012). Sedimentary evolution of lake van (Eastern Turkey) reconstructed from high-resolution seismic investigations. *International Journal of Earth Sciences*, 102(2), 571-585. doi:10.1007/s00531-012-0816-x
- Cukur, D., Krastel, S., Schmincke, H., Sumita, M., Çağatay, M. N., Meydan, A. F., Stockhecke, M. (2014). Seismic stratigraphy of lake van, eastern Turkey. *Quaternary Science Reviews*, 104, 63-84. doi:10.1016/j.quascirev.2014.07.016
- Çağatay, M., Öğretmen, N., Damcı, E., Stockhecke, M., Sancar, Ü., Eriş, K., Özeren, S. (2014). Lake level and climate records of the last 90ka from the northern basin of lake van, eastern Turkey. *Quaternary Science Reviews*, 104, 97-116. doi:10.1016/j.quascirev.2014.09.027
- Degens, E. T., & Kurtman, F. (1978). *The Geology of Lake Van*. Ankara: MTA Press.

- Fan, Z., Li, X., Li, Z., Ma, W., Zhu, Z., Li, J., Dong, Y. (2024). Geochemical behavior of shallow buried nodules from clarion–clipperton fracture zone in the east pacific: a la-icp-ms mapping analysis perspective. *Minerals*, 14(1), 80. <https://doi.org/10.3390/min14010080>
- Haraguchi, A. (2012). Phosphorus is released from sediments in a riparian community at the estuary of the Chikugogawa River in western Japan. *American Journal of Plant Sciences*, 03(07), 962-970. <https://doi.org/10.4236/ajps.2012.37114>
- Harrison, A. L., Dipple, G. M., Song, W., Power, I. M., Mayer, K. U., Beinlich, A., Sinton, D. (2017). Changes in mineral reactivity driven by pore fluid mobility in partially wetted porous media. *Chemical Geology*, 463, 1-11. <https://doi.org/10.1016/j.chemgeo.2017.05.003>
- Khosravi, R., Zarej, M., Bigalke, M. (2018). Characterizing major controls on spatial and seasonal variations in the chemical composition of surface and pore brine of Maharlu Lake, southern Iran. *Aquatic Geochemistry*, 24(1), 27-54. <https://doi.org/10.1007/s10498-018-9329-y>
- Koehler, G., Wassenaar, L. I., Hendry, M. J. (2000). An automated technique for measuring δd and $\delta 18o$ values of porewater by direct co_2 and h_2 equilibration. *Analytical Chemistry*, 72(22), 5659–5664. <https://doi.org/10.1021/ac000498n>
- Landmann, G., Reimer, A., Kempe, S. (1996a). Climatically induced lake level changes at Lake Van, Turkey, during the Pleistocene/Holocene transition. *Global Biogeochemical Cycles*, 10(4), 797-808. doi:10.1029/96gb02347
- Landmann, G., Reimer, A., Lemcke, G., Kempe, S. (1996b). Dating late glacial abrupt climate changes in the 14,570-year long continuous varve record of Lake Van, Turkey. *Paleogeography, Palaeoclimatology, Palaeoecology*, 122(1-4), 107-118. doi:10.1016/0031-0182(95)00101-8
- Lemcke, G., Sturm, M. (1997). $\delta 18o$ and trace element measurements as a proxy for the reconstruction of climate changes at Lake Van (Turkey): Preliminary results. *Third Millennium BC Climate Change and Old World Collapse*, 653-678. doi:10.1007/978-3-642-60616-8_29

- Litt, T., Krastel, S., Sturm, M., Kipfer, R., Örcen, S., Heumann, G., Niessen, F. (2009). 'PALEOVAN', International Continental Scientific Drilling Program (ICDP): Site survey results and perspectives. *Quaternary Science Reviews*, 28(15-16), 1555-1567. doi:10.1016/j.quascirev.2009.03.002
- Litt, T., Pickarski, N., Heumann, G., Stockhecke, M., Tzedakis, P. C. (2014). A 600,000-year-long continental pollen record from Lake Van, eastern Anatolia (Turkey). *Quaternary Science Reviews*, 104, 30-41. doi:10.1016/j.quascirev.2014.03.017
- Mann, Michael (2003). Little Ice Age. *Encyclopedia of Global Environmental Change, The Earth System: Physical and Chemical Dimensions of Global Environmental Change*. (eds. MacCracken, Michael C.; Perry, John S.) Vol. 1. John Wiley & Sons.
- Mattei, A., Goblet, P., Barbecot, F., Guillon, S., Coquet, Y., Wang, S. (2020). Can soil hydraulic parameters be estimated from the stable isotope composition of pore water from a single soil profile? *Water*, 12(2), 393. <https://doi.org/10.3390/w12020393>
- Meydan, A. F., Akkol, S., Doğan, O. H. (2022). Implications from the meteorological data affect water level fluctuations of the lake van (Eastern Anatolia/Türkiye). *Marine Science and Technology Bulletin*, 11(3), 299-308. doi:10.33714/masteb.1125161
- Pickarski, N., Litt, T. (2017). A new high-resolution pollen sequence at Lake Van, Turkey: Insights into penultimate interglacial–glacial climate change on vegetation history. *Climate of the Past*, 13(6), 689-710. doi:10.5194/cp-13-689-2017
- Pickarski, N., Kwiecien, O., Djamali, M., Litt, T. (2015). Vegetation and environmental changes during the last interglacial in eastern Anatolia (Turkey): A new high-resolution pollen record from Lake Van. *Paleogeography, Palaeoclimatology, Palaeoecology*, 435, 145-158. doi:10.1016/j.palaeo.2015.06.015
- Poletaeva, V., Tirskikh, E., Pastukhov, M. (2021). Hydrochemistry of sediment pore water in the Bratsk Reservoir (Baikal region, Russia). *Scientific Reports*, 11(1). <https://doi.org/10.1038/s41598-021-90603-x>

- Rao, S., Mogili, N. V., A, P., A, L. (2020). Aqueous chemistry of anthropogenically contaminated Bengaluru lakes. *Sustainable Environment Research*, 30(1). doi:10.1186/s42834-020-00049-5
- Rasmussen, P., Sonnenborg, T., Gonciar, G., Hinsby, K. (2013). Assessing impacts of climate change, sea level rise, and drainage canals on saltwater intrusion to the coastal aquifer. *Hydrology and Earth System Sciences*, 17(1), 421-443. <https://doi.org/10.5194/hess-17-421-2013>
- Stockhecke, M., Anselmetti, F. S., Meydan, A. F., Odermatt, D., Sturm, M. (2012). The annual particle cycle in Lake Van (Turkey). *Paleogeography, Palaeoclimatology, Palaeoecology*, 333-334, 148-159. doi:10.1016/j.palaeo.2012.03.022
- Stockhecke, M., Kwiecien, O., Vigliotti, L., Anselmetti, F. S., Beer, J., Çağatay, M. N., Channel, J. E., Kipfer, R., Lachner, J., Litt, T., Pickarski, N., Sturm, M. (2014). Chronostratigraphy of the 600,000-year-old continental record of Lake Van (Turkey). *Quaternary Science Reviews*, 104, 8-17. doi:10.1016/j.quascirev.2014.04.008
- Sturm, K., Yuan, Z., Gibbes, B., Ulrich, W., Grinham, A. (2014). Methane and nitrous oxide sources and emissions in a subtropical freshwater reservoir, southeast Queensland, Australia. *Biogeosciences*, 11(18), 5245-5258. <https://doi.org/10.5194/bg-11-5245-2014>
- Tomonaga, Y., Brennwald, M. S., Livingstone, D. M., Kwiecien, O., Randlett, M., Stockhecke, M., Kipfer, R. (2017). Porewater salinity reveals past lake-level changes in Lake Van, the earth's largest soda lake. *Scientific Reports*, 7(1). doi:10.1038/s41598-017-00371-w
- Wick, L., Lemcke, G., Sturm, M. (2003). Evidence of Lateglacial and Holocene climatic change and human impact in eastern Anatolia: High-resolution pollen, charcoal, isotopic and geochemical records from the laminated sediments of Lake Van, Turkey. *The Holocene*, 13(5), 665-675. doi:10.1191/0959683603hl653rp
- Zhu, Q. and Aller, R. C. (2012). Two-dimensional dissolved ferrous iron distributions in marine sediments as revealed by a novel planar optical sensor. *Marine Chemistry*, 136-137, 14-23. <https://doi.org/10.1016/j.marchem.2012.04.002>

CHAPTER 3
DIAGNOSIS OF HEALTHY AND MALIGNANT
HUMAN ENDOMETRIUM TISSUE SAMPLES
BY FTIR AND RAMAN SPECTRA

Assoc.Prof.Dr.Deniz Türköz ALTUĞ¹

Prof.Dr. Kemal Kürşat BOZKURT²

Prof.Dr. Evrim ERDEMOĞLU³

DOI: <https://dx.doi.org/10.5281/zenodo.14503503>

¹ Süleyman Demirel University, Faculty of Education, Department of Science Education, East Campus, Isparta, Turkey. ORCID: 0000-0002-1861-6263

² Süleyman Demirel University, Faculty of Medicine, Department of Medical Pathology, Isparta, Turkey. ORCID: 0000-0003-1522-9388

³ Süleyman Demirel University, Faculty of Medicine, Department of Gynecologic Oncology, Isparta, Turkey. ORCID: 0000-0002-5993-6968

1. INTRODUCTION

The use of molecular spectroscopy methods, which both Raman and infrared spectroscopy, are increasing as an effective tool in cancer research. This label-free and noninvasive methodology reveals biomarkers typical of many types of cancer by elucidating their malignancy characteristics (Bangaoil, et al., 2020).

In recent years, especially the kits used for the diagnosis of diseases are expensive, the diagnosis of diseases in a long time, the development of new and alternative methods of diagnosis is a subject of great interest. The use of spectroscopic methods in the diagnosis of various diseases in the literature shows an increasing trend recently.

There are many studies on this subject. For example, normal and malignant human gastric tissue samples were evaluated for 30 patient tissues using both FTIR and the mathematical model (Ghassemi, et al., 2021). FTIR spectrums were also used for the detection of cervical cancer in Thai women (Sindhuphak, et al., 2003). It was showed that pancreatic cancer can be diagnosed using FTIR, Raman and analytical algorithms (Szymoński, et al., 2021). It was showed that FTIR-ATR and Raman spectroscopy are a potential diagnostic method especially in the 1800-700 cm^{-1} (finger print) region in the diagnosis of lung cancer (Bangaoil, et al., 2020) (Lewis, et al., 2010) (Huang, et al., 2003). Wan et al gastrointestinal neoplasms have reviewed many studies as a Review article and suggested that it can be used for diagnosis (Wan, Wang, & Zhang, 2017). Gajjar et al show that IR and/or Raman spectroscopy has the potential to provide a new diagnostic approach in brain tumors (Gajjar, et al., 2013). Paraskevaidi et al. stated in their study that they obtained accurate and effective results using FTIR and data analysis methods for diagnostic ovarian cancer (Paraskevaidi, et al., 2018). Kumar et al and Hubbard et al have shown that FTIR and Raman spectroscopy methods can be used for breast cancer diagnosis in the future (Kumar, Desmedt, Larsimont, Sotiriou, & Goormaghtigh, 2013) (Hubbard, Dudgeon, Ferguson, Shore, & Stone, 2021). Caber et al. showed that FTIR Spectroscopy as a Potential Non-Invasive Screening Tool for Pediatric Precursor B Lymphoblastic Leukemia (Chaber, et al., 2021). Depciuch et al. suggested that FTIR and Raman spectroscopy can be used in the diagnosis of endometrial cancer, but more

studies are needed to prove this (Depciuch, et al., 2021). Albayrak and Gazi et al concluded that chemometric-assisted FTIR spectroscopy method is a fast, simple, reliable and environmentally friendly method and can be used as an important alternative to histopathological methods in the diagnosis of cancerous and normal prostate tissues (Albayrak, 2018) (Gazi, et al., 2006). In the study of Yang et al., chemometric studies and FTIR spectroscopy were compared for the diagnosis of liver cancer, and it was decided that it is a method that can be used in the diagnosis of this disease (Zang, Ou, Yang, Shi, & Liu, 2021). The results obtained by scanning Cancer together with the keywords, Raman and, FTIR in WOS database between the years 2011-2021 are presented graphically in Figure 1.

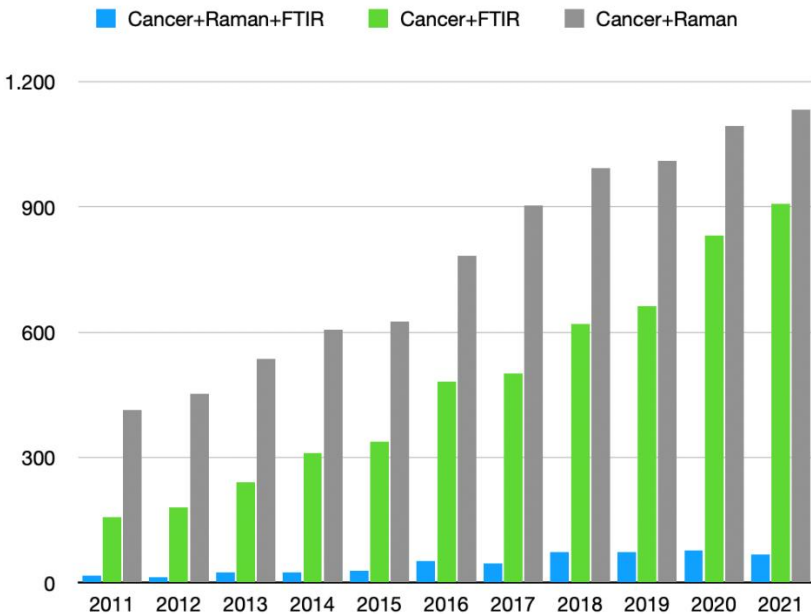


Figure 1: The results of according to WOS database numerical data of Cancer, Raman and FTIR

According to this graph, while there are many studies for cancer and Raman in recent years, the number of studies for cancer, Raman and, FTIR are very few. It is seen that the use of both Raman and FTIR spectroscopic methods in cancer studies has recently started to attract attention and it is being studied with an increasing trend beside it has just started to be studied.

This study is an additional study to other studies that prove that it can be performed with molecular spectroscopic methods in a very short time and inexpensively, instead of providing the diagnosis of cancerous cells with an average of 8-10 days of research with normal pathological methods. Because the usability of a method in ordinary life, the more studies there are, the more reliable it is. We tried to support the literature on this issue.

Permission was obtained from the SDU Faculty of Medicine Ethics Committee to conduct the study with the decision numbered 335 and dated 30.11.2022.

2.EXPERIMENTAL

For this study, samples taken from endometrial surgery performed in SDU Research and Practice Hospital were turned into general paraffin blocks. Histological features of the samples: 2 samples taken from healthy and endometrioid type endometrial cancer tissue of a single patient. Then, malignant, and healthy tissues cut at a thickness of 20 μm by a pathologist were separated and fixed on loaded slides. First, the samples were kept in drying oven at 60°C for 1 hour to ensure that the paraffin on the sample melted as much as possible. Then, for the deparaffinization process, the samples, which were bathed in xylene 2 times for 10 minutes, were ensured to get rid of the paraffin thoroughly. Again, dehydration was ensured thanks to 2 alcohol baths for 10 minutes and finally the samples were dipped in acetone and left to dry at room temperature. Thus, it was made ready for FTIR and Raman spectroscopy.

FTIR (The Fourier Transform Infrared Spectroscopy) has been used to record the spectra of the samples with Jasco FT/IR-4700 spectrometer in range of 4000-400 cm^{-1} , using ATR technique in SDÜ (Süleyman Demirel University), YETEM (Innovative Technologies Application and Research Center), Isparta, Türkiye.

The RAMAN measurements were obtained by using Thermo scientific-DXR2 Raman Microscope, working with a laser wavelength of 532 nm in SDÜ-SUDUM (Natural Products Application and Research Center), Isparta, Türkiye.

3.RESULT AND DISCUSSION

FTIR spectroscopic examinations can be used in the diagnosis of cancerous tissues. FTIR can show not only spectra from proteins or DNA/RNA in a cell, but also spectral features from any metabolite present. These properties have been demonstrated in the work of Kumar et al. (Kumar, Desmedt, Larsimont, Sotiriou, & Goormaghtigh, 2013).

FTIR and Raman spectroscopic images taken for healthy and malignant endometrial tissues are shown in Figure 2.

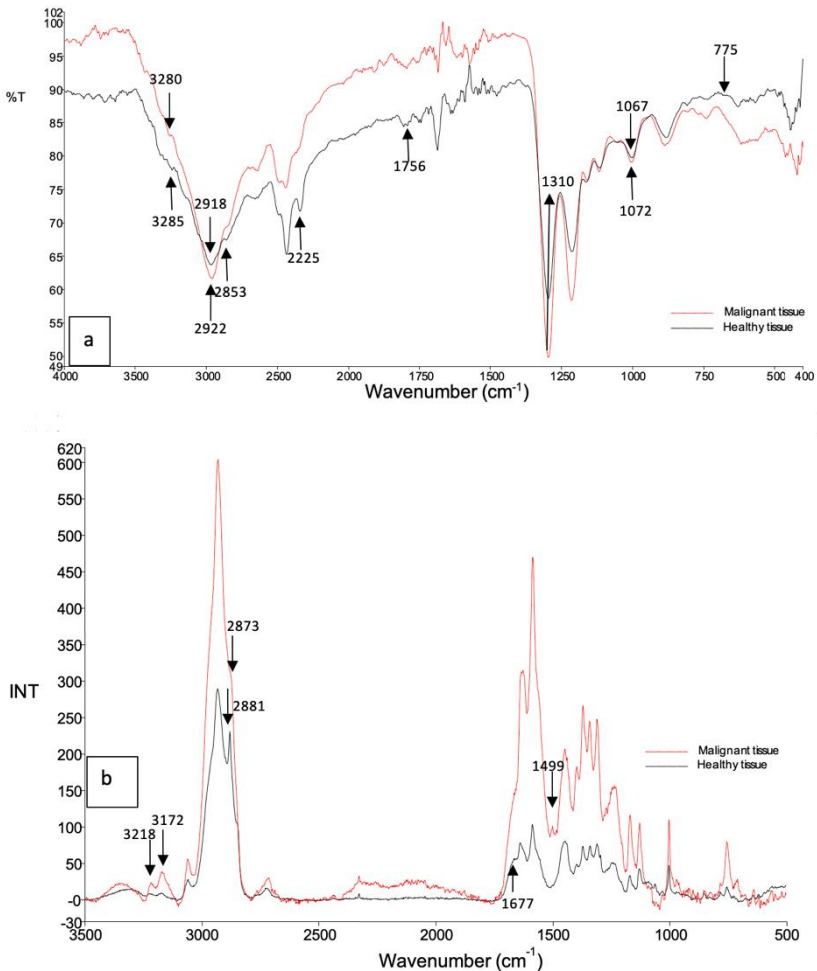


Figure 2: (a) FTIR and (b) Raman Spectra of healthy and malignant endometrium tissues

In FTIR and Raman spectrum examinations, newly formed peaks, shifts in peaks and disappearing peaks were evaluated compared to healthy tissue. The data obtained are presented in Table 1.

Table 1: Assignments of FTIR and Raman Spectra of healthy and malignant endometrium tissues

Assignments	FTIR (cm ⁻¹)		Raman (cm ⁻¹)		References
	Malignant tissue	Healthy tissue	Malignant tissue	Healthy tissue	
N-H stretching	3280	3285			(Chaber, et al., 2021) (Barth & Zscherp, 2002)
NH ₂ , O-H stretching			3218		(Zhang, et al., 2022)
NH, CH ₃ stretching			3172		(Zhang, et al., 2022)
Anti-symmetric C-H stretching in CH ₂	2922	2918			(Chaber, et al., 2021) (Zang, Ou, Yang, Shi, & Liu, 2021)
Symmetric C-H stretching in CH ₃			2881	2873	(Depciuch, et al., 2021) (Zang, Ou, Yang, Shi, & Liu, 2021)
Anti-symmetric and symmetric C-H stretches from proteins and lipids		2853			(Zang, Ou, Yang, Shi, & Liu, 2021) (Su & Lee, 2020)
Carbonyl group of peptide linages		2225			(Dong, Huang, Zhao, Sampath, & Caughey, 1994)
C=O stretching		1756			(Huang, et

of lipids					al., 2003) (Gajjar, et al., 2013)
C=O stretching of Amid I				1677	(Huang, et al., 2003) (Gajjar, et al., 2013) (Depciuch, et al., 2021)
Amide I and II groups in peptide linkages of proteins			1499		(Su & Lee, 2020)
Coupling C-N stretching and N-H bending in amide III bands	1310	1310			(Chaber, et al., 2021) (Zang, Ou, Yang, Shi, & Liu, 2021) (Barth & Zscherp, 2002)
Anti-symmetric and symmetric C-O and P-O areas in DNA, RNA and phospholipids	1072	1067			(Chaber, et al., 2021) (Su & Lee, 2020)
Symmetric breathing, tryptophan		775			(Huang, et al., 2003)

The peak at 3285 cm^{-1} , which is thought to belong to the N-H vibration and seen in healthy tissue, was observed at 3280 cm^{-1} in malignant tissue with a shift of about 5 cm^{-1} . The peak at 2918 cm^{-1} , which is thought to have an anti-symmetric C-H vibration in CH_2 , was observed shifting to 2922 cm^{-1} . The peak at 1067 cm^{-1} observed in healthy tissue shifts to 1072 cm^{-1} in malignant tissue. It is thought that all these shifts are caused by new bonds and interactions formed in the malignant tissue. Because newly formed bonds will change the bond lengths and bond angles between atoms when they interact with healthy tissue, this can cause shifts in the FTIR spectra.

Vibration bands observed at 2853, 2225, 1756, and 775 cm^{-1} observed in healthy tissue were not observed in malignant tissue. These vibrations, which are not observed in the FTIR spectra, prove that there are molecular changes in the malignant tissue.

When the Raman spectra are examined, unlike healthy tissue, peaks occur clearly at 3218 and 3172 cm^{-1} in malignant tissue. These peaks related to the protein structure can be assigned as N-H stretching vibration and $\text{NH}_2/\text{O-H}$ symmetric stretching vibration, respectively. These designations agree with the work of Zhang et al. (Zhang, et al., 2022).

The band observed clearly at 2881 cm^{-1} in healthy tissue is observed as a weak vibration band in malignant tissue and as a shifted 2873 cm^{-1} shoulder vibration band. The band at 1677 cm^{-1} observed in healthy tissue is not seen in malignant tissue. The new weak peaks observed in 3218, 3171 and 1499 cm^{-1} in the malignant tissue prove that new formations have occurred in the molecular structure.

When the FTIR and Raman spectra were compared, almost all the newly formed vibration bands were observed in the Raman spectra. In the FTIR spectra, on the other hand, the disappearing vibration bands and shifts are observed more intensely. The reason for this is that even if new bands are formed in the FTIR spectra, the overlapping bands, which we call overtones, may prevent the newly formed bands from being observed. Therefore, it was concluded that Raman spectroscopy would be more appropriate if newly formed bands were to be examined.

4.CONCLUSION

As a result of the spectroscopic examinations, spectroscopic changes were observed between the malignant and the healthy tissues. In particular, these changes are the emergence of new peaks in both the FTIR spectrum and the Raman spectrum in malignant tissue and the shift of the peaks relative to the healthy tissue peak. This proves the existence of new formations in molecular terms. Therefore, spectral analysis methods are considered promising for the diagnosis of malignant tissue. Additionally, the use of this

method in future studies can be carried out in multiple samples.

REFERENCES

- Albayrak, M. (2018). Investigation of the Usability of Fourier Transform Infrared Spectroscopy in Diagnosis of Prostate Cancer. *Journal of the Institute of Science and Technology*, 8(4), 223-227.
- Bangaol, R., Santillan, A., Angeles, L. M., Abanilla, L., Lim Jr, A., Ramos, M. C., . . . Albano, P. M. (2020). ATR-FTIR spectroscopy as adjunct method to the microscopic examination of hematoxylin and eosin-stained tissues in diagnosing lung cancer. *Plos one*, 15(5: e0233626.), 1-15.
- Barth, A., & Zscherp, C. (2002). What vibrations tell about proteins. *Quarterly reviews of biophysics*, 35(4), 369-430.
- Chaber, R., Kowal, A., Jakubczyk, P., Arthur, C., Łach, K., Wojnarowska-Nowak, R., . . . Cebulski, J. (2021). A Preliminary Study of FTIR Spectroscopy as a Potential Non-Invasive Screening Tool for Pediatric Precursor B Lymphoblastic Leukemia. *Molecules*, 26(4: 1174), 1-13.
- Depciuch, J., Barnaś, E., Skręt-Magierło, J., Skręt, A., Kaznowska, E., Łach, K., . . . Cebulski, J. (2021). Spectroscopic evaluation of carcinogenesis in endometrial cancer. *Scientific reports*, 11(1), 1-12.
- Dong, A., Huang, P., Zhao, X. J., Sampath, V., & Caughey, W. S. (1994). Characterization of sites occupied by the anesthetic nitrous oxide within proteins by infrared spectroscopy. *Journal of Biological Chemistry*, 269(39), 23911-23917.
- Gajjar, K., Heppenstall, L. D., Pang, W., Ashton, K. M., Trevisan, J., Patel, I. I., . . . Martin, F. L. (2013). Diagnostic segregation of human brain tumours using Fourier-transform infrared and/or Raman spectroscopy coupled with discriminant analysis. *Analytical Methods*, 5(1), 89-102.
- Gazi, E., Baker, M., Dwyer, J., Lockyer, N. P., Gardner, P., Shanks, J. H., . . . Brown, M. D. (2006). A correlation of FTIR spectra derived from prostate cancer biopsies with Gleason grade and tumour stage. *European urology*, 50(4), 750-761.
- Ghassemi, M., Barzegari, S., Hajian, P., Zham, H., Mirzaei, H. R., & Shirazi, F. H. (2021). Diagnosis of normal and malignant human gastric tissue

- samples by FTIR spectra combined with mathematical models. *Journal of Molecular Structure*, 1229(129493), 1-10.
- Huang, Z., McWilliams, A., Lui, H., McLean, D. I., Lam, S., & Zeng, H. (2003). Near-infrared Raman spectroscopy for optical diagnosis of lung cancer. *International journal of cancer*, 107(6), 1047-1052.
- Hubbard, T. J., Dudgeon, A. P., Ferguson, D. J., Shore, A. C., & Stone, N. (2021). Utilization of Raman spectroscopy to identify breast cancer from the water content in surgical samples containing blue dye. *Translational Biophotonics*, 3(2: e202000023), 1-8.
- Kumar, S., Desmedt, C., Larsimont, D., Sotiriou, C., & Goormaghtigh, E. (2013). Change in the microenvironment of breast cancer studied by FTIR imaging. *Analyst*, 138(14), 4058-4065.
- Lewis, P. D., Lewis, K. E., Ghosal, R., Bayliss, S., Lloyd, A. J., Wills, J., . . . Mur, L. A. (2010). Evaluation of FTIR spectroscopy as a diagnostic tool for lung cancer using sputum. *BMC cancer*, 10(1), 1-10.
- Paraskevaidi, M., Morais, C. L., Lima, K. M., Ashton, K. M., Stringfellow, H. F., Martin-Hirsch, P. L., & Martin, F. L. (2018). Potential of mid-infrared spectroscopy as a non-invasive diagnostic test in urine for endometrial or ovarian cancer. *Analyst*, 143(13), 3156-3163.
- Sindhuphak, R., Issaravanich, S., Udomprasertgul, V., Srisookho, P., Warakamin, S., Sindhuphak, S., . . . Dusitsin, N. (2003). A new approach for the detection of cervical cancer in Thai women. *Gynecologic oncology*, 90(1), 10-14.
- Su, K. Y., & Lee, W. L. (2020). Fourier transform infrared spectroscopy as a cancer screening and diagnostic tool: a review and prospects. *Cancers*, 12(115), 1-19.
- Szymoński, K., Lipiec, E., Sofińska, K., Skirlińska-Nosek, K., Milian-Ciesielska, K., Szpor, J., . . . Szymoński, M. (2021). Spectroscopic screening of pancreatic cancer. *Clinical Spectroscopy*, 3(100016), 1-4.
- Wan, Q. S., Wang, T., & Zhang, K. H. (2017). Biomedical optical spectroscopy for the early diagnosis of gastrointestinal neoplasms. *Tumor Biology*, 39(7-1010428317717984), 1-12.

- Zang, X., Ou, Q., Yang, W., Shi, Y., & Liu, G. (2021). Diagnosis of liver cancer by FTIR spectra of serum. *Spectrochimica Acta Part A: Molecular and Biomolecular Spectroscopy*, 263(120181), 1-7.
- Zhang, L., Zhou, Y., Wu, B., Zhang, S., Zhu, K., Liu, C.-h., . . . Alfano, R. R. (2022). Intraoperative detection of human meningioma using a handheld visible resonance Raman analyzer. *Lasers in Medical Science*, 37, 1311–1319.

CHAPTER 4

**SYNTHESIS OF NOVEL FLUORESCENT TRIAZOLE
DERIVATIVE AND INVESTIGATION OF ITS ELECTRONIC
PROPERTIES**

Prof.Dr. Ayşegül GÜMÜŞ¹

Prof. Dr. Selçuk GÜMÜŞ²

DOI: <https://dx.doi.org/10.5281/zenodo.14503511>

¹ Bartin University, Faculty of Science, Department of Biotechnology, Bartin, Turkey, agumus@bartin.edu.tr, 0000-0002-1613-7074

² Bartin University, Engineering, Architecture and Design Faculty, Department of Basic Sciences, Bartin, Turkey, sgumus@bartin.edu.tr, 0000-0002-8628-8943

1. INTRODUCTION

Heterocyclic compounds hold significant importance across various fields, including chemistry, biology, medicine, and industry (Welsch et al., 2010; Fryatt et al., 2004; Michael, 2008). The design and synthesis of straightforward heterocyclic molecules for metal ion detection are particularly valuable due to the numerous advantages of this approach. These include simplicity, exceptional sensitivity, high efficiency, selectivity, cost-effectiveness, notable specificity, ease of use, and the capability for real-time monitoring (Lee et al., 2016; Ghorai et al., 2016; Kose et al., 2015).

Fluorescent sensors can detect specific metal ions with high sensitivity and selectivity, making them valuable tools in environmental monitoring, biological studies, and industrial applications. Fluorescent sensors for metals are formed by integration of two critical components: Metal chelating or binding moiety which selectively binds metal ions, ensuring specificity and strong interaction with the target metal and fluorophore capable of absorbing light at a specific wavelength and re-emitting it at a longer wavelength, providing the fluorescent signal (Carter et al., 2014).

Triazoles are five-membered heterocyclic compounds containing three nitrogen atoms, existing in two isomeric forms: 1,2,3-triazole and 1,2,4-triazole. The synthesis of 1,2,3-triazole derivatives has garnered significant attention due to their wide-ranging applications in chemical and bioactive materials science due to their favorable properties, such as hydrogen bonding capability, rigidity, moderate dipole character, and metabolic stability. A key method for synthesizing these compounds is the Huisgen 1,3-dipolar cycloaddition, where organic azides react with alkynes to form a mixture of regioisomers, 1,4- and 1,5-disubstituted 1,2,3-triazoles (Huisgen, 1963). However, this classical reaction has limitations, including high temperature requirements, long reaction times, poor selectivity, and difficulties in separating regioisomers.

A breakthrough came when Meldal and Sharpless (2001-2002) introduced Cu(I) catalysis, which transformed the reaction into a highly efficient process under mild conditions, selectively yielding only the 1,4-regioisomer with minimal purification (Meldal et. al., 2002 and Kolb et. al.,

2001). This innovation, known as “click chemistry,” has enabled the synthesis of structurally diverse 1,2,3-triazoles with applications in various fields such as bioactive compounds, chemotherapeutic agents, agrochemicals, photostabilizers, and metal chelators (Huisgen, 1984, Agalave et. al., 2011, Krivopalov et. al., 2005 and Yet, 2004).

Pyrene is widely recognized as a highly effective fluorophore for ratiometric sensors due to its remarkable photophysical properties, including unique fluorescence behavior and sensitivity to environmental changes (Gandhi et. al., 2018). Its long fluorescence lifetime allows for detailed time-resolved studies, while its high quantum yield ensures efficient emission, making it highly suitable for sensitive detection. Furthermore, the extended π -electron delocalization in its structure contributes to strong fluorescence and makes it capable of interacting with a variety of analytes. Additionally, pyrene exhibits exceptional chemical and thermal stability, which enhances its durability and reliability in various sensor applications. These attributes collectively make pyrene an indispensable component in the design of advanced ratiometric sensing systems.

Quinoline is a prominent nitrogen-based heterocycle widely studied for its extensive applications in medicinal, bioorganic, industrial, and synthetic organic chemistry (Matada et al., 2021). Recently, quinoline-based derivatives have garnered significant attention in fluorescence sensing due to their distinctive spectroscopic properties and large conjugated molecular structures (Gao et al., 2013; Weng et al., 2009; Meng et al., 2012). Known for their strong fluorescence, these compounds are ideal for fluorescence-based applications, with tunable emission properties achieved through structural modifications, enabling the development of sensors with tailored emission wavelengths.

Molecular conjugation encompasses techniques employed in pharmacology, advanced materials, and nanotechnology to connect two molecular entities. Over the last twenty years, click chemistry has revolutionized the field by providing innovative and efficient approaches to molecular recognition.

In this context, our objective was to synthesize styrylquinoline-pyrene conjugate linked through a triazole bridge, as well as to analyze their three-dimensional geometries and gather insights into its electronic properties (Figure 1). Moreover, interaction of this compound with metal cations was investigated with TDDFT computations.

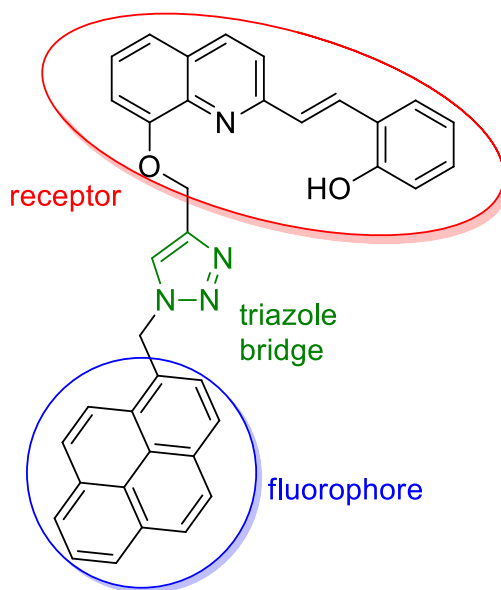
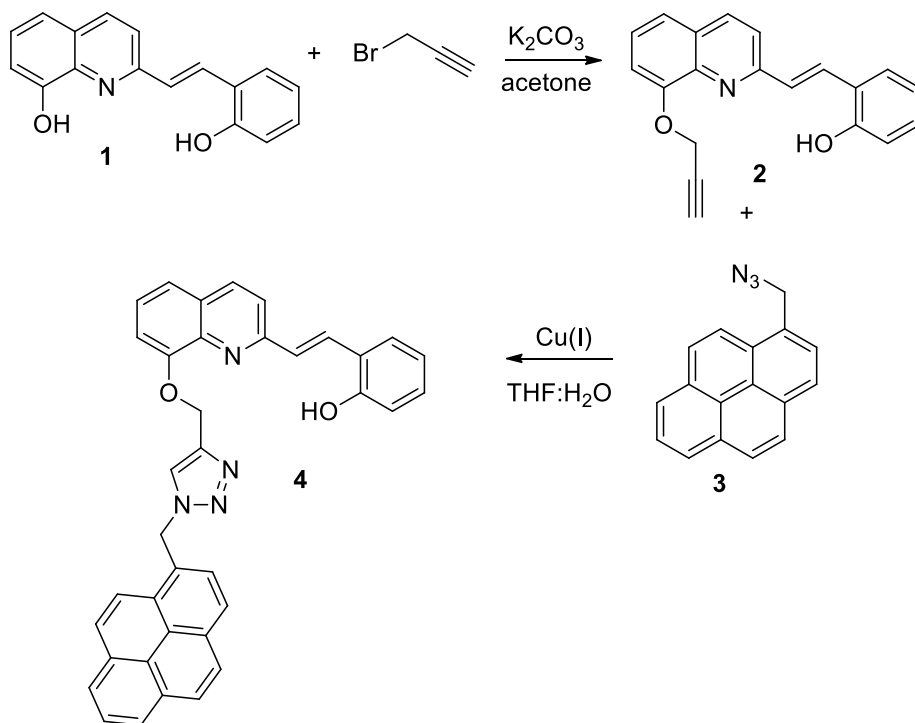


Figure 1. Styrylquinoline-triazole-pyrene derivative

2. RESULTS AND DISCUSSION

Introducing substituents like styryl groups into the hydroxyquinoline ligand system improves the thermal stability of metal complexes relative to unsubstituted quinoline complexes and enhances their solubility in organic solvents. For this reason, styrylquinoline derivative was chosen as starting material for the synthesis of target triazole compound, **4** in main two steps as shown in Scheme 1. Initially, OH group on quinoline part of (E)-2-(2-hydroxystyryl)quinolin-8-ol **1** was propargylated with propargyl bromide in the presence of potassium carbonate as a base in acetone at room temperature (Gümüş et al., 2023).

1-(azidomethyl)pyrene derivative was prepared by the reaction of 1-(bromomethyl)pyrene with NaN_3 in DMSO. The key intermediate, compound **2**, was then treated with azidomethylpyrene, **3** in accordance with a copper(I)-mediated click cycloaddition reaction in 4:1 THF/ H_2O solvent mixture to afford product **4**. All the new compounds were well characterized by ^1H and ^{13}C NMR and mass spectroscopies.



Scheme 1. Synthesis of target compound, **4**.

In addition to synthesizing the target compound experimentally, we have also performed theoretical calculations on it and its complexes. Density Functional Theory has been used to compute some structural and electronic properties of the compounds at the B3LYP/6-31++G(d,p) level of theory.

The three-dimensional ground state (S_0) geometries of the compound was optimized using Density Functional Theory (DFT) (Kohn and Sham, 1965) with the Gaussian 16W software package (Frisch et al., 2016). The

hybrid functional B3LYP was used in the calculations. B3LYP incorporates Becke's three-parameter exchange functional (B3) (Becke, 1988) and the nonlocal correlation functional of Lee, Yang, and Parr (LYP) (Lee et al., 1988). These functionals are empirically parameterized with constraints based on the uniform electron gas model, allowing the method to handle dispersion forces effectively, a limitation in standard DFT approaches (Zhao and Truhlar, 2006, 2008; Karton, et al., 2008).

Vibrational analyses were conducted using the same basis sets as in the geometry optimizations. The absence of imaginary frequencies confirmed that compound's structure corresponds to at least a local minimum on the potential energy surface. Standard mode analysis was performed for the $3N-6$ vibrational degrees of freedom, where N represents the number of atoms in the molecule.

To determine the compound's minimum energy geometries, both the low-energy triplet (T) and singlet (S) excited states were optimized. Vertical excitation energies and oscillator strengths for the lowest singlet and triplet transitions were calculated using Time-Dependent DFT (TD-DFT) with various hybrid functionals and basis sets at the optimized ground-state geometries. The electronic absorption spectra, including maximum absorption wavelengths, oscillator strengths, and primary configuration assignments, were derived from these TD-DFT calculations.

In addition to the experimental synthesis of the target compound, we have conducted theoretical calculations on compound **4**. Using Density Functional Theory at the B3LYP/6-31++G(d,p) level, we computed several structural and electronic properties of the compound.

The optimized 3D geometry revealed that the triazole unit extends outward from the central cavity, allowing for complexation with metal cations (Figure 2).

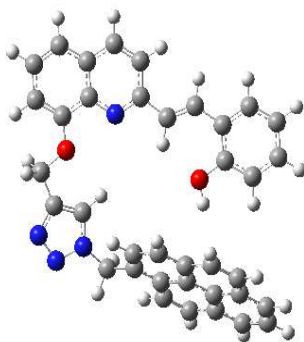


Figure 2. Geometry optimized structure of target compound 4.

Subsequently, we conducted a scan coordinate computation to confirm the stability of the compound, ensuring that it represents a global minimum rather than just a local minimum on the potential energy surface. The results of the scan showed that the triazole unit pointing outward is more stable than when it points inward into the cavity. This preference is likely due to not only steric effects but also interactions such as π - π or π -lone pair electron interactions between the pyrene moiety and the nitrogen of the amine group (Figure 3).

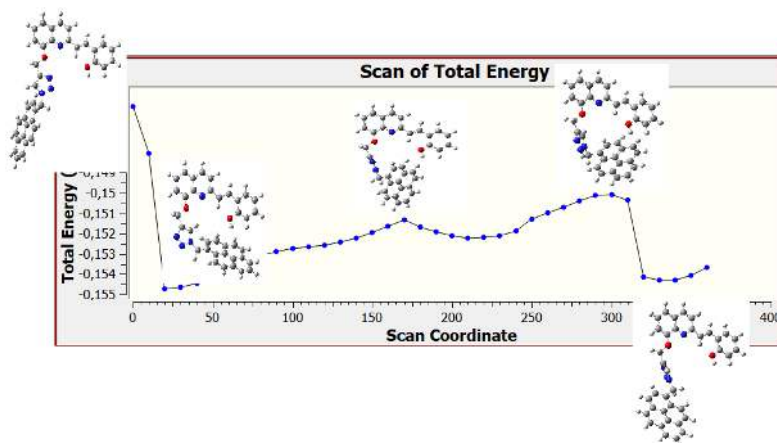


Figure 3. Dihedral angle scanning for 4.

The molecular electrostatic potential map is a useful tool for identifying regions of electron localization in a complex system. Electronegative atoms or strongly electron-withdrawing or donating groups influence the electron distribution across the structure. This map helps predict areas in the structure that are prone to nucleophilic attack or electrophilic interactions. Electron-rich regions, such as those in our case, are particularly favorable for cation chelation.

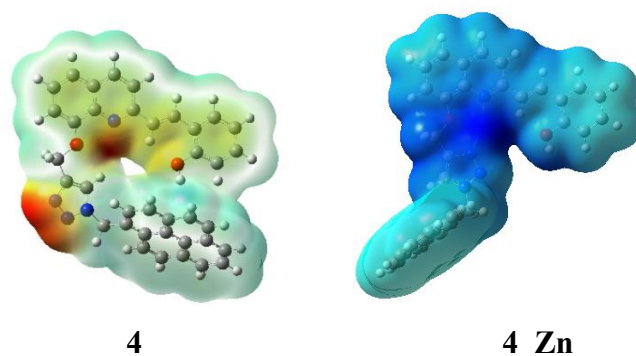


Figure 4. Molecular electrostatic potential maps of **4** and **4_Zn**

The 3D electrostatic potential maps of **4** and **4_Zn**, shown in Figure 4, clearly demonstrate that the electron distribution of the parent compound is significantly altered upon chelation with Zn^{2+} . The electron deficiency of the cation is compensated by electron donation from the nitrogen lone pairs of the triazole and quinoline units, resulting in a more uniform electron distribution after metal cation interaction. In addition to the changes in electron distribution, the complexation also induces notable structural changes. The triazole unit rotates inward into the complexation cavity to participate in chelation.

Another key factor influencing the structural and electronic properties is the HOMO and LUMO orbitals. In the parent molecule, the HOMO is located on the quinoline part and the LUMO on the pyrene part, whereas in the complex, the HOMO is on pyrene, and the LUMO is primarily located on the metal, as expected, since the LUMO represents electron-deficient sites. The energy gap between HOMO and LUMO is also crucial in determining

whether the compound behaves as an insulator, conductor, or semiconductor. The parent structure can be considered an insulator or, at best, a semiconductor, whereas the complex exhibits conductive properties with a HOMO-LUMO energy gap (ΔE) of only 1.31 eV (Figure 5).

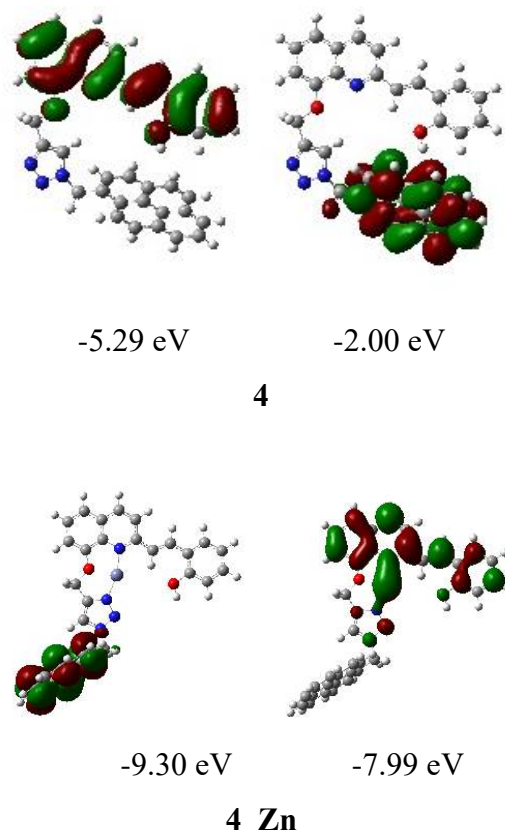
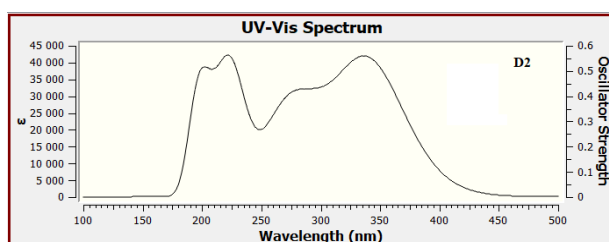


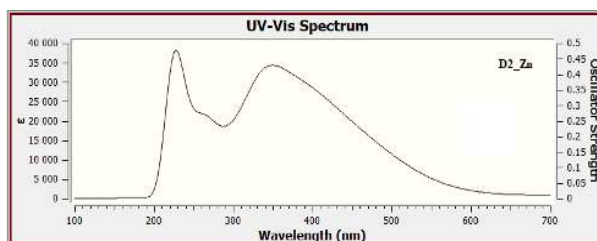
Figure 5. HOMO and LUMO orbital schemes of **4** and **4_Zn**.

As a result of metal coordination, the electronic properties of the structure undergo significant changes. One way to observe and confirm this change is by calculating the absorption spectra using Time-Dependent Density Functional Theory (TDDFT). The TDDFT calculations were performed with the B3LYP/6-31++G(d,p) method, considering 100 excitation levels to generate the UV-VIS spectra. The absorption spectrum of the **4**

structure shows two broad bands at 220 nm and 340 nm (Figure 6), along with two shoulder bands at 200 nm and 270 nm. Upon coordination with Zn^{2+} , these two broad bands are replaced by a single, very broad band in the absorption spectrum. Additionally, the sharpest band disappears, and a red shift is observed in the remaining bands. The red shift could be attributed to the reduced HOMO-LUMO energy gap, which results from the metal's contribution to the conductivity of the structure. Furthermore, both shoulder bands vanish upon complexation.



4



4_Zn

Figure 6. UV-VIS spectra for 4 and 4_Zn.

3. EXPERIMENTAL

3.1. Monopropargylation of E-2-(2-hydroxystyryl)quinolin-8-ol

(E)-2-(2-hydroxystyryl)quinolin-8-ol (263 mg, 1 mmol) was dissolved in 10 mL of acetone. K_2CO_3 (276 mg, 2 mmol) was added and stirred under reflux for 30 min. Propargyl bromide (0.11 mL, 1 mmol) was then added to the mixture and stirred at reflux overnight. The reaction was terminated by monitoring by TLC. After the mixture was cooled, it was filtered and the solvent was removed. The product **2** was purified by column

chromatography using silica gel and EtOAc/hexane (1:4) (Gümüş et al., 2023).

White solid. (271 mg, 90% yield); ^1H NMR (CDCl_3 , 400 MHz): δ 8.10 (d, $J=8.6$ Hz, 1H, Ar-H), 8.06 (d, $J=16.5$ Hz, 1H, CH), 7.75-7.72 (m, 1H, Ar-H), 7.69 (d, $J=8.6$ Hz, 1H, Ar-H), 7.42-7.37 (m, 2H, Ar-H), 7.35-7.31 (m, 1H, CH), 7.29 (dd, $J=8.2$ Hz and $J=1.2$, 1H, Ar-H), 7.16 (dd, $J=7.6$ Hz and $J=1.2$, 1H, Ar-H), 7.09-8.05 (m, 2H, Ar-H), 4.84 (s, 1H, CH_2O), 4.83 (s, 1H, CH_2O), 2.56 (t, $J=2.4$ Hz, 1H, CH); ^{13}C NMR (CDCl_3 , 100 MHz): δ 155.5, 154.1, 152.1, 138.0, 136.2, 129.7, 129.1, 128.9, 127.4, 127.3, 127.2, 126.2, 121.9, 120.3, 117.6, 112.9, 110.0, 78.5, 75.8, 56.4. LC-MS/MS. Anal. Calcd for $\text{C}_{20}\text{H}_{15}\text{NO}_2$ $[\text{M}+\text{H}]^+$: m/z 302.1176. Found: m/z 302.1176.

3.2. Synthesis of 1-(azidomethyl)pyrene

1-(Bromomethyl)pyrene (500 mg, 1,69 mmol), sodium azide (164 mg, 2,54 mmol) ve 3 mL DMF were mixed at 60 °C for 6 h. Reaction mixture was cooled and 20 mL water was added. Then, water phase was extracted with Et_2O . Organic phase was dried with MgSO_4 and solvent was evaporated (Gümüş et al., 2022).

Yellow solid. (395 mg, 91% yield). ^1H NMR (CDCl_3 , 400 MHz): δ 8.20-8.17 (m, 3H, Ar-H), 8.13-8.09 (m, 3H, Ar-H), 8.06-7.99 (m, 3H, Ar-H), 7.91 (d, $J=7.8$ Hz, 1H, Ar-H), 4.96 (s, 2H, CH_2N). ^{13}C NMR (CDCl_3 , 100 MHz): δ 131.7, 131.2, 130.7, 129.1, 128.3, 128.2, 127.8, 127.4, 127.3, 126.1, 125.6, 125.5, 124.9, 124.6, 124.5, 122.6, 53.0.

3.3. (E)-2-(2-(8-((1-(pyren-1-ylmethyl)-1H-1,2,3-triazol-4-yl)methoxy) quinolin-2-yl)vinyl)phenol, 4

(E)-2-(2-(8-(prop-2-yn-1-yloxy)quinolin-2-yl)vinyl)phenol (150 mg, 0.5 mmol) and azidomethylpyrene (134 mg, 0.5 mmol) was dissolved in 5 mL of THF: H_2O (4:1). $\text{CuSO}_4 \cdot 5\text{H}_2\text{O}$ (13 mg, 0.5 mmol) and sodium ascorbate (20 mg, 0.1 mmol) were added and the solution was stirred at room temperature for 24 hours. After the experiment was terminated, water was added to the mixture and extraction was performed with EtOAc. The product was purified by column chromatography using EtOAc:Hexane (1:2).

Yellow solid. (181 mg, 65% yield). mp 187-190 °C; (^1H NMR (CDCl_3 , 400 MHz): δ 8.20-8.17 (m, 2H, Ar-H), 8.15-8.13 (m, 1H, Ar-H), 8.06-8.02 (m, 3H, Ar-H), 8.00-7.95 (m, 2H, Ar-H), 7.90 (d, $J=7.8$ Hz, 1H, Ar-H), 7.84 (d, $J=16.5$ Hz, 1H, CH), 7.80 (d, $J=8.7$ Hz, 1H, Ar-H), 7.56 (dd, $J=7.7$ and $J=1.6$ Hz, 1H, Ar-H), 7.43 (s, 1H, Ar-H), 7.41-7.37 (m, 1H, Ar-H), 7.33 (d, $J=8.6$ Hz, 1H, Ar-H), 7.25-7.16 (m, 4H, Ar-H, CH), 7.03-7.00 (m, 1H, Ar-H), 6.98-6.94 (m, 1H, Ar-H), 6.22 (s, 2H, CH_2N), 5.21 (s, 2H, CH_2O); ^{13}C NMR (CDCl_3 , 100 MHz): δ 156.1, 153.9, 151.9, 144.4, 136.1, 132.1, 131.1, 130.5, 129.9, 129.2, 129.0, 128.2, 127.7, 127.3, 127.2, 127.1, 127.1, 126.6, 126.3, 125.9, 125.9, 125.8, 125.0, 124.9, 124.4, 122.7, 121.8, 121.6, 120.1, 117.6, 113.4, 110.1, 63.0, 52.5. LC-MS/MS. Anal. Calcd $\text{C}_{37}\text{H}_{26}\text{N}_4\text{O}_2$ $[\text{M}+\text{H}]^+$: m/z 559.2128. Found: m/z 559.2141. IR ν_{max} (neat cm^{-1}): 3407, 3045, 2920, 1597, 1452, 1041, 839, 750, 701.

4. CONCLUSION

In conclusion, stryloquinoline as a good receptor unit was connected to pyrene skeleton by azide-alkyne cycloaddition constructing the triazole bridge and novel fluorescent compound was obtained in good yield.

Theoretical calculations using the B3LYP/6-31++G(d,p) level of theory were performed to obtain structural and electronic data for the target compound and its Zn^{2+} complex. In the initial geometry, the triazole unit pointed outward from the central cavity, but it rotated towards the complexation site, interacting with the cation to form a chelate. The molecular electrostatic potential maps indicated effective complexation, as the charge distribution of the molecule was significantly altered upon interaction with the metal cation. Negative charge on some electronegative atoms was redistributed towards the cation, resulting in a more uniform charge distribution. The contribution of atoms and groups to the frontier molecular orbitals also changed due to complex formation. In the final complex structure, the LUMO is primarily localized on the Zn atom. Finally, the absorption spectra for 4 and 4_Zn were calculated using the same method, showing that some absorption bands of the target structure disappeared while new bands appeared after complexation.

ACKNOWLEDGEMENT

We are grateful to the Turkish Scientific and Technical Research Council (TUBITAK) for the grant (No. 118Z421).

REFERENCES

- Agalave, S. G., Maujan, S. R., Pore, V. S. (2011). Click chemistry: 1,2,3-triazoles as pharmacophores. *Chem. Asian J.*, 6, 2696–2718.
- Becke AD. Density-functional exchange-energy approximation with correct asymptotic behavior. *Phys Rev A* 1988, 38, 3098–3100.
- Carter, K. P., Young, A. M., Palmer, A. E. (2014). Fluorescent Sensors for Measuring Metal Ions in Living Systems. *Chem. Rev.*, 114, 4564–4601.
- Frisch, M. J., Trucks, G. W., Schlegel, H. B., Scuseria, G. E., Robb, M. A., Cheeseman, J. R., Scalmani, G., Barone, V., Petersson, G. A., Nakatsuji, H., Li, X., Caricato, M., Marenich, A. V., Bloino, J., Janesko, B. G., Gomperts, R., Mennucci, B., Hratchian, H. P., Ortiz, J. V., Izmaylov, A. F., Sonnenberg, J. L., Williams-Young, D., Ding, F., Lipparini, F., Egidi, F., Goings, J., Peng, B., Petrone, A., Henderson, T., Ranasinghe, D., Zakrzewski, V. G., Gao, J., Rega, N., Zheng, G., Liang, W., Hada, M., Ehara, M., Toyota, K., Fukuda, R., Hasegawa, J., Ishida, M., Nakajima, T., Honda, Y., Kitao, O., Nakai, H., Vreven, T., Throssell, K., Montgomery, Jr., J. A., Peralta, J. E., Ogliaro, F., Bearpark, M. J., Heyd, J. J., Brothers, E. N., Kudin, K. N., Staroverov, V. N., Keith, T. A., Kobayashi, R., Normand, J., Raghavachari, K., Rendell, A. P., Burant, J. C., Iyengar, S. S., Tomasi, J., Cossi, M., Millam, J. M., Klene, M., Adamo, C., Cammi, R., Ochterski, J. W., Martin, R. L., Morokuma, K., Farkas, O., Foresman, J. B., & Fox, D.J. (2016) Gaussian, Inc., Wallingford CT.
- Fryatt, T., Pettersson, H. I., Gardipee, W. T., Bray, K. C., Green, S. J., Slawin, A. M. Z., Beall, H. D., Moody, C. (2004). Novel quinolinequinone antitumor agents: structure-metabolism studies with NAD(P)H:quinone oxidoreductase (NQO1), *Bioorg. Med. Chem.*, 12, 1667–1687.
- Gandhi, S., Iniya, M., Anand, T., Kotla, N. G., Sunnapu, O., Singaravadi, S., Gulyani, A., Chellappa, D. (2018). Chemically diverse small molecule fluorescent chemosensors for copper ion. *Coord. Chem. Rev.*, 357, 50-104.

- Gao, C., Jin, X., Yan, X., An, P., Zhang, Y., Liu, L.L., Tian, H., Liu, W., Yao, X., Tang, Y. (2013). A small molecular fluorescent sensor for highly selectivity of zinc ion, *Sens. Actuators B*, 176, 775–781.
- Ghorai, A., Mondal, J., Chowdhury, S., Patra, G.K. (2016). Solvent-dependent fluorescent-colorimetric probe for dual monitoring of Al^{3+} and Cu^{2+} in aqueous solution: an application to bio-imaging, *Dalton Trans.* 45, 11540–11553.
- Gümüş, A., Gümüş, S. (2022). Synthesis of Quinoline-Pyrene Derivatives and Theoretical Investigation of Their Fluorescence and Electronic Properties. *ChemistrySelect*, 7, 202203958.
- Gümüş, A., Sadeghian, N., Sadeghi, M., Taslimi, P., & Gümüş, S. (2023). Novel triazole bridged quinoline-anthracene derivatives: synthesis, characterization, molecular docking, evaluation of electronic and enzyme inhibitory properties. *Journal of Biomolecular Structure and Dynamics*, 1–16.
- Huisgen R. (1963). 1,3-dipolar cycloadditions. Past and future. *Angew Chem Int Ed.* 2, 565-598.
- Huisgen, R. (1984). 1,3-Dipolar Cycloaddition—Introduction, Survey, Mechanism. In *1,3-Dipolar Cycloaddition Chemistry*. Padwa, A., Ed. Wiley: New York.
- Karton A, Tarnopolsky A, Lamre JF, Schatz GC, Martin JML. Highly Accurate First-Principles Benchmark Data Sets for the Parametrization and Validation of Density Functional and Other Approximate Methods. Derivation of a Robust, Generally Applicable, Double-Hybrid Functional for Thermochemistry and Thermochemical Kinetics. *J. Phys. Chem. A*, 2008, 112 (50), pp 12868–12886.
- Kohn W, Sham LJ. Self-consistent equations including exchange and correlation effects. *Phys. Rev.* 1965, 140, 1133-1138.
- Kolb H. C., Finn M. G., Sharpless K. B. (2001). Click Chemistry: Diverse Chemical Function from a Few Good Reactions. *Angew Chem Int Ed.* 40(11), 2004-2021.
- Kose, M., Purtas, S., Gungor, S.A., Ceyhan, G., Akgun, E., McKee, V. (2015). A novel Schiff base: Synthesis, structural characterisation and comparative sensor studies for metal ion detections, *Spectrochim. Acta A* 136, 1388–1394.

- Krivopalov, V. P., Shkurko, O. P. (2005), 1,2,3-Triazole and its derivatives. Development of methods for the formation of the triazole ring. *Russian Chem. Rev.*, 74, 339–379.
- Lee C, Yang W, Parr RG, Development of the Colle–Salvetti correlation energy formula into a functional of the electron density. *Phys Rev B* 1988, 37, 785–789.
- Lee, S. Y., Lee, J. J., Bok, K.H., Kim, S.Y., Kim, C. (2016). Highly selective and sensitive colorimetric chemosensor for detection of Co^{2+} in a near-perfect aqueous solution, *RSC Adv.* 6 28081–28088.
- Matada, B. S., Pattanashettar, R., Yernale, N. G. (2021). A comprehensive review on the biological interest of quinoline and its derivatives, *Bioorganic & Medicinal Chemistry*, Vol. 32, 115973-115998.
- Meng, X.M., Wang, S.X., Li, Y.M., Zhu, M.Z., Guo, Q.X. (2012). 6-Substituted quinoline-based ratiometric two-photon fluorescent probes for biological Zn^{2+} detection, *Chem. Commun.* 48, 4196–4198.
- Meldal C. W., Tornøe C., Meldal M. (2002). Peptidotriazoles on Solid Phase: [1,2,3]-Triazoles by Regiospecific Copper(I)-Catalyzed 1,3-Dipolar Cycloadditions of Terminal Alkynes to Azides. *J Org Chem.* 67(9), 3057-3064.
- Meng, X.M., Wang, S.X., Li, Y.M., Zhu, M.Z., Guo, Q.X. (2012). 6-Substituted quinoline-based ratiometric two-photon fluorescent probes for biological Zn^{2+} detection, *Chem. Commun.* 48, 4196–4198.
- Michael, J. P. (2008). Quinoline, quinazoline and acridonealkaloids, *Nat. Prod. Rep.* 25, 166–187
- Welsch, M. E., Snyder, S. S., Stockwell, B. R. (2010). Privileged scaffolds for library design and drug discovery, *Curr. Opin. Chem. Biol.* Vol. 14, No. 3, 347-361.
- Weng, Y., Chen, Z. L., Wang, F., Xue, L., Jiang, H. (2009). High sensitive determination of zinc with novel water-soluble small molecular fluorescent sensor, *Anal. Chim. Acta* 647, 215–218.
- Yet, L. (2004). *Progress in Heterocyclic Chemistry*; Elsevier, Oxford, UK.
- Zhao Y, Truhlar DG. The M06 suite of density functionals for main group thermochemistry, thermochemical kinetics, noncovalent interactions, excited states, and transition elements: two new functionals and

systematic testing of four M06-class functionals and 12 other functionals. *Theor Chem Acc* 2008, 120, 215-241.

Zhao Y, Truhlar DG. Density Functional for Spectroscopy: No Long-Range Self-Interaction Error, Good Performance for Rydberg and Charge-Transfer States, and Better Performance on Average than B3LYP for Ground States. *J Phys Chem A* 2006, 110, 13126-13130.

Zhao Y, Truhlar DG. A new local density functional for main-group thermochemistry, transition metal bonding, thermochemical kinetics, and noncovalent interactions. *J Chem Phys* 2006, 125, 194101-194118.

CHAPTER 5

TADF PROPERTIES OF NOVEL D- π -A TYPE OLEDs

Prof. Dr. Selçuk GÜMÜŞ¹

Prof.Dr. Ayşegül GÜMÜŞ²

DOI: <https://dx.doi.org/10.5281/zenodo.14503517>

¹ Bartın University, Engineering, Architecture and Design Faculty, Department of Basic Sciences, Bartın, Turkey, sgumus@bartin.edu.tr, 0000-0002-8628-8943

² Bartın University, Faculty of Science, Department of Biotechnology, Bartın, Turkey, agumus@bartin.edu.tr, 0000-0002-1613-7074

1. INTRODUCTION

Lighting systems account for approximately 19% of global electricity consumption. Lighting technology is among the fastest-evolving fields, and researchers have long been focused on reducing electricity usage in this area. Modern advancements have led to the development of devices like Light Emitting Diodes (LEDs), which consume about 95% less energy than traditional Edison bulbs while producing bright light. LEDs have gained significant popularity due to their efficiency and versatility. Additionally, newer technologies, such as Organic Light Emitting Diodes (OLEDs), offer the potential for thinner, lighter, and more flexible surfaces, combining aesthetics with functionality. Research and development in OLED technology continue, promising both enhanced usability and innovative design solutions.

The availability of various organic materials and the ability to tailor their properties through chemical modifications make them simpler and more cost-effective to work with compared to inorganic materials. Their versatility in processing through different methods has significantly contributed to the prominence of OLED technology. The foundation of this field dates back to 1953 when Bernanose and colleagues, followed by Pope and colleagues in 1963, created the first organic electroluminescent cells. These advancements led to the design of light-emitting diodes (OLEDs) using light-emitting polymers.

Light, as a physical phenomenon, stimulates the human eye's nerves to create the sensation of vision, though the visible portion of the electromagnetic spectrum is relatively small. Humans can perceive wavelengths ranging from deep violet (400 nm) to deep red (750 nm). The hue of light varies based on its frequency and wavelength, requiring an excitation energy between 1.8 and 3.1 eV to emit visible wavelengths (Kalyani et al., 2017).

Light production in nature occurs via two mechanisms: incandescence and luminescence. Incandescence involves the emission of light due to heat energy, where atoms or molecules at high temperatures release thermal vibrations as electromagnetic radiation. The sun is the most prominent example, providing the heat and light necessary for life on Earth through

incandescence. In contrast, luminescence emits light without heat, arising from electron transitions within a material from high to low energy states. This process can be triggered by photon absorption, chemical or biological interactions, subatomic particles, radiation, or mechanical stress on a crystal. The emitted light's wavelength is determined by the luminescent material itself (Fourassier, 1984; McKeever, 1985).

Fluorescence, discovered experimentally in 1852, is the immediate emission of light at a longer wavelength after absorbing light at a specific wavelength (e.g., blue light absorption leading to yellow light emission). This phenomenon occurs over a short duration known as the fluorescence lifetime, during which excited electrons return to their ground state, releasing excess energy as photons. The system's electronic multiplicity remains unchanged during fluorescence transitions (Sparks et al., 2014).

In contrast, phosphorescence involves delayed emission, resulting from forbidden energy state transitions. Since triplet-singlet transitions are less likely than singlet-singlet transitions, phosphorescence occurs over longer durations (Kalyani et al., 2017). The Jablonski diagram (Figure 1) illustrates fluorescence and phosphorescence mechanisms. According to Reinhoudt's empirical criterion, intersystem crossing (ISC) is efficient when the energy gap between S1 and T1 states is below 0.6 eV for all ligands (deSa et al., 2000).

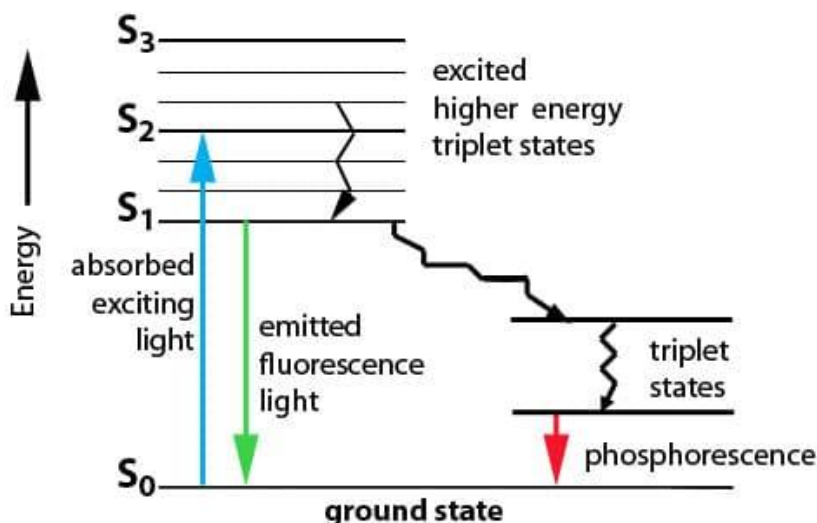


Figure 1. Simplified diagram showing fluorescence and phosphorescence.

LEDs have been in use for nearly 50 years, but until about a decade ago, their application was limited to indicator lamps in electrical devices. Their adoption surged due to their exceptional efficiency, high reliability, robust design, and the absence of toxic metals. Over time, advancements in LED technology enabled brighter LEDs, expanding their applications to include general and decorative lighting, traffic signals, electronic billboards, car headlights, flashlights, cameras, store signs, vehicle destination displays, and more. Recent developments have also incorporated organic materials into LEDs, further improving their performance.

Organic Light Emitting Diode (OLED) technology represents a significant evolution in lighting. OLEDs are unconventional light sources that could replace traditional lighting systems. They consist of carbon-based films sandwiched between two charged electrodes—typically a metallic cathode and a transparent anode, often made of glass (Binggeli, 2012). The organic layers include an emissive layer, electron-transport layer, hole-injection layer, and hole-transport layer (Tsai et al., 2014). These structures consume less energy while producing brighter light (Liu et al., 2014; Zhang et al., 2002; Xiaoxiao et al., 2014).

OLED technology was first developed by Eastman Kodak in the early 1980s. It is now replacing LCDs in portable devices such as PDAs and smartphones due to its superior power efficiency, lighter weight, faster response times, higher brightness, and thinner profile. Additionally, OLEDs offer better contrast, lower production costs, and reduced power consumption compared to LCDs (Patel and Prajapati, 2014).

When an electric field is applied to an OLED, electrons travel through the lowest unoccupied molecular orbital (LUMO), while holes move through the highest occupied molecular orbital (HOMO). These charges combine with emitter molecules, creating triplet or singlet excitons. In the emissive layer of the OLED, the recombination of positive and negative charges under voltage produces electroluminescent light. Unlike LCDs, which modulate transmitted or reflected light, OLED displays are emissive devices that generate their own light (Kalyani et al., 2017).

In this study, a series of anthracene-based compounds (Figure 2), were designed and their structural and electronic properties analyzed using Density Functional Theory. These donor-acceptor (D- π -A) compounds show potential for applications in organic solar cells, OLEDs, and fluorescent organic materials.

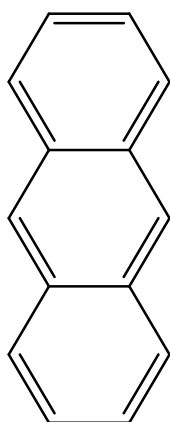


Figure 2. Structure of the parent compound (anthracene)

2. METHOD OF CALCULATION

The three-dimensional ground state (S_0) geometries of all compounds were optimized using Density Functional Theory (DFT) (Kohn and Sham, 2015) with the Gaussian 16W software package (Frisch et al., 2016). The hybrid functionals B3LYP and CAM-B3LYP were employed in the calculations. B3LYP integrates Becke's three-parameter exchange functional (B3) (Becke, 1988) and the nonlocal correlation functional of Lee, Yang, and Parr (LYP) (Lee et al., 1988). These functionals are parameterized empirically with constraints based on the uniform electron gas model (Zhao and Truhlar, 2006, 2008; Karton et al., 2008), enabling the method to address dispersion forces effectively, a notable limitation in standard DFT approaches.

Vibrational analyses were performed using the same basis sets employed in the geometry optimizations. The absence of imaginary frequencies in the vibrational studies confirmed that each compound's structure corresponds to at least a local minimum on the potential energy surface. Standard mode analysis was conducted for the $3N-6$ vibrational degrees of freedom, where N represents the number of atoms in the molecule.

To identify the compounds' minimum energy geometries, the low-energy triplet (T) and singlet (S) excited states were optimized. Using Time-Dependent DFT (TD-DFT) with various hybrid functionals and basis sets, vertical excitation energies and oscillator strengths for the lowest singlet and triplet transitions were calculated at the optimized ground-state geometries (Casida et al., 1998). The electronic absorption spectra, including maximum absorption wavelengths, oscillator strengths, and primary configuration assignments, were derived from these TD-DFT calculations.

While a few exceptions were noted, literature evidence suggests that excitation energy predictions using PBE0, wB97XD, and CAM-B3LYP functionals align most closely with experimental data (Yanez et al., 2017). Accordingly, TD-DFT computations were conducted using B3LYP/6-311++G(d,p) methods, and the results were compared.

3. RESULTS AND DISCUSSION

The pursuit of sustainable, large-scale energy generation has driven the search for innovative concepts and applications, particularly those utilizing cost-effective, environmentally friendly materials with abundant availability and diversity. Organic semiconductor materials, in contrast to their inorganic counterparts like silicon, are less expensive and offer the potential for creating thin, flexible devices due to their exceptionally high optical absorption coefficients.

For fluorescent molecules, the radiative exciton fraction is typically around 0.25 (Baldo et al., 1999; Segal et al., 2003). However, introducing phosphorescent emitters can increase this value up to 1 (Baldo et al., 1998; Wilson et al., 2001; Sun et al., 1999). This improvement comes at the cost of using rare metals such as iridium or platinum, which facilitate efficient spin-orbit coupling (Adachi et al., 2001; O'Brien et al., 1999; Baldo et al., 1999), potentially raising the production costs of OLED devices. The classical external quantum efficiency (EQE) limits for OLEDs using fluorescent and phosphorescent emitters are approximately 5% and 20%, respectively. Recently, a novel approach—converting non-radiative triplet states into radiative singlet states—has emerged as a way to surpass these limits (Meerholz and Müller, 2001).

Thermally Activated Delayed Fluorescence (TADF) emitters have attracted significant attention, leading to the development of numerous new compounds exhibiting this behavior (Endo et al., 2009, 2011; Czerwiec and Yersin, 2011; Leitl et al., 2013). TADF works by reducing the energy gap (ΔE_{ST}) between the lowest excited singlet (S_1) and triplet (T_1) states (Figure 3). This is achieved by spatially separating the highest occupied molecular orbital (HOMO) and the lowest unoccupied molecular orbital (LUMO), allowing reverse intersystem crossing (RISC) to convert triplet excitons into singlet excitons via a thermally induced mechanism (Boltzmann statistics). This process, often referred to as singlet harvesting, enhances OLED fluorescence efficiency by increasing the radiative exciton fraction (Endo et al., 2011), enabling EQE values that exceed classical limits and approach those of systems employing phosphorescent emitters (Leitl et al., 2013).

A small ΔE_{ST} minimizes electron-electron repulsion in the triplet state by reducing the overlap integral between the wave functions of the molecule's ground and excited states (Endo et al., 2009). In this framework, the HOMO represents the ground state, while the LUMO corresponds to the excited state. Localizing HOMO and LUMO electron densities on donor and acceptor groups, respectively, is an effective strategy to reduce wave function overlap. This effect is further enhanced by steric separation achieved through spiro junctions or bulky substituents between the donor and acceptor units (Endo et al., 2011).

Building on these insights, this study proposes a series of donor-acceptor (D- π -A) anthracene-based derivatives, as potential TADF emitters (Figure 2). The parent compound, Anthracene is a solid polycyclic aromatic hydrocarbon (PAH) of formula $C_{14}H_{10}$, consisting of three fused benzene rings. It is a component of coal tar. Anthracene is used in the production of the red dye alizarin and other dyes. Anthracene is colorless but exhibits a blue (400–500 nm peak) fluorescence under ultraviolet radiation. (Lindsey, et al. 2014).

In this work, anthracene was modified to obtain 16 new compounds by addition of π link (benzene, thiophene and furan) together with electronwithdrawing groups (cyano groups or cyano group containing organic groups) (Figure 3). The concept originated from extensive spectroscopic studies of the parent pyrazine compound (Khodae et al., 2012; Nishida et al., 2004; Ivanov et al., 2006). By integrating the strong withdrawing groups properties of anthracene with various acceptor units, this work aims to design novel TADF-active compounds.

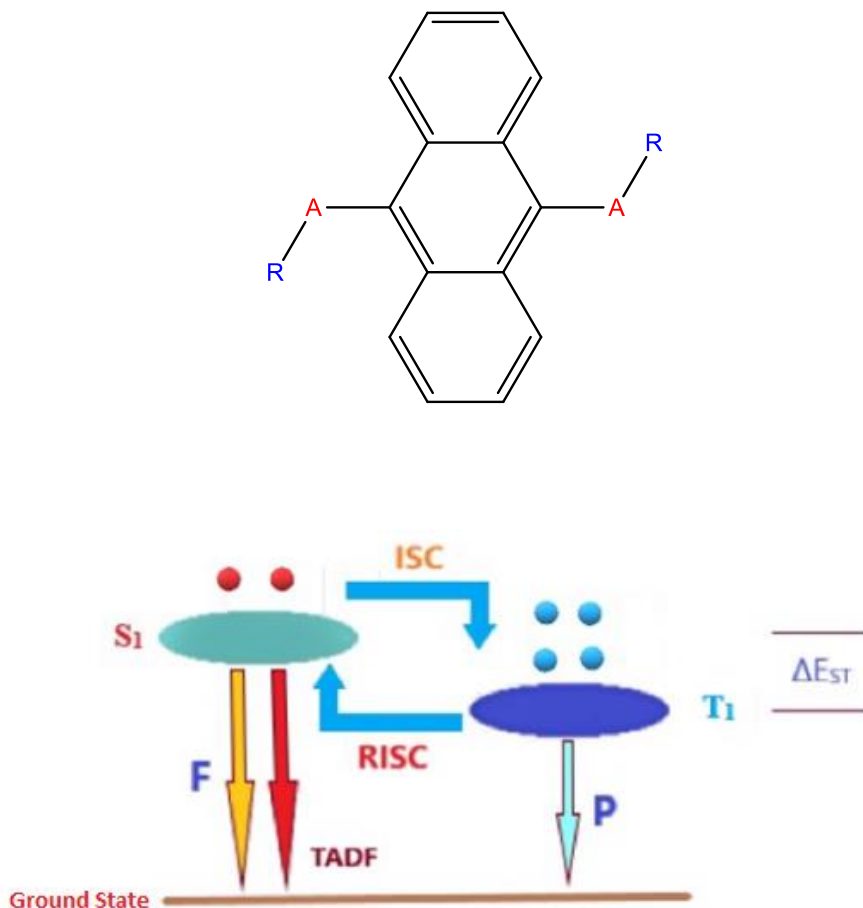


Figure 3. Structures of potential TADF compounds

3.1. Semiconductor Properties

The conjugation of π -electrons forms the basis of the electronic structure in all organic semiconductors. In a conjugated organic system, single and double carbon-carbon bonds alternate. Single bonds, associated with localized electrons, are referred to as σ -bonds, while double bonds consist of both a σ -bond and a π -bond. The π -electrons are delocalized due to the overlap of π orbitals along the conjugation pathway, allowing them to move between carbon atoms. The Lowest Unoccupied Molecular Orbital (LUMO)

corresponds to the unoccupied π -bands, while the Highest Occupied Molecular Orbital (HOMO) represents the occupied π -bands. Organic semiconductors have band gaps (E) ranging from 0.5 to 4 eV (Atkins et al., 2006).

The geometry-optimized structures of the new compounds are illustrated in Figure 4. Frontier molecular orbital energies were calculated using the B3LYP/6-311+G(d,p) method, with the results presented in Table 1. All computed band gap (ΔE) values were found to be below 4 eV. As expected, incorporating donor units with acceptors reduces the inter-frontier molecular orbital energy gap by extending the conjugation path. The parent compound (A) exhibited a band gap of 3.70 eV, which decreased with the addition of donor units. Consequently, all the compounds show potential for use as semiconducting materials, with the smallest band gaps observed in compounds 10 and 15.

Figures 4 and 5 depict the geometry-optimized structures and 3D frontier molecular orbital energy diagrams of the compounds, respectively. These diagrams provide insights into the compounds' reactivity. The LUMO indicates the Lewis acidity of the system, while the HOMO reflects its basicity. Consequently, studying the frontier molecular orbitals is critical, as they determine the reactive centers within the molecules. Understanding which atoms contribute to these orbitals is equally important.

For the compounds to be effective candidates for thermally activated delayed fluorescence (TADF), they must exhibit a clear separation between HOMO and LUMO, ensuring low exchange energy. This separation can be achieved through steric hindrance, which induces twisting between donor and acceptor units (Nakagawa et al., 2012; Mehes et al., 2012; Nasu et al., 2013). In donor-acceptor (D-A) structures, the HOMOs are primarily localized on the donor moieties (Figure 5), while the LUMOs are predominantly found on the acceptor core, composed of pyrazine and strongly electron-withdrawing cyano groups. The significant dihedral angles (approximately 25–90°) between the donor units and the phenanthrene-pyrazine core with cyano groups result in a distinct spatial separation of the HOMO and LUMO orbitals. This separation

ensures that the HOMO is concentrated on the donor regions and the LUMO on the acceptor regions of the system.

Table 1. Results of computations (All data are in eV)

Compound	DFT			TD-DFT (ΔE_{ST})
	B3LYP/6-311++(d,p)			B3LYP
	HOMO	LUMO	ΔE	6-311++(d,p)
A	-6.80	-3.10	3.70	0.65
1	-5.36	-2.99	2.37	0.47
2	-5.88	-3.19	2.81	0.12
3	-5.54	-3.52	2.02	0.11
4	-5.50	-3.00	2.50	0.09
5	-4.94	-2.94	2.00	0.08
6	-5.26	-2.45	2.81	0.47
7	-5.69	-2.96	2.73	0.12
8	-6.02	-3.02	3.00	0.11
9	-5.26	-3.04	2.18	0.09
10	-4.78	-2.86	1.92	0.10
11	-6.05	-2.76	4.29	0.12
12	-5.67	-3.32	2.35	0.18
13	-5.71	-3.07	2.64	0.25
14	-5.69	-3.04	2.65	0.41
15	-4.47	-2.56	1.91	0.02
16	-5.98	-2.72	3.26	0.65

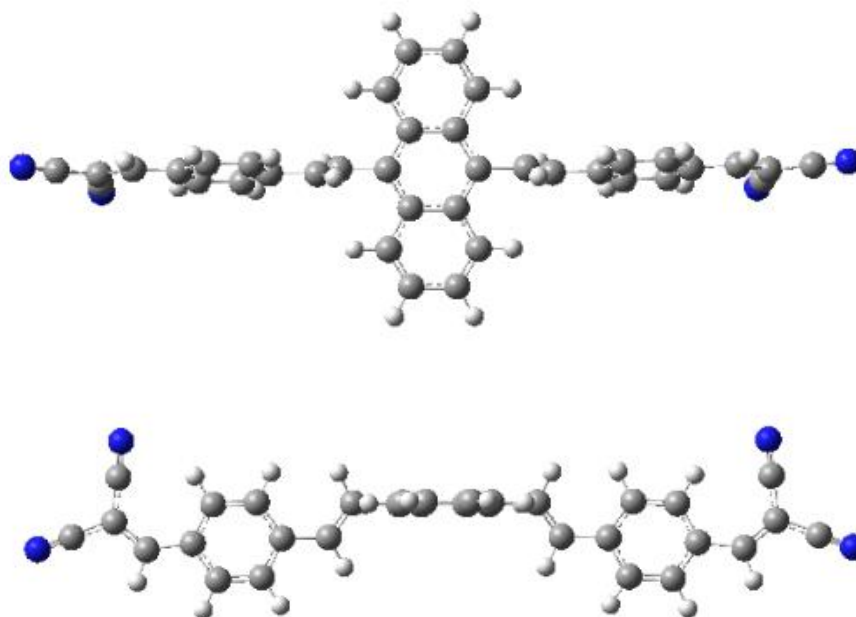


Figure 4. Geometry optimized structure of one of the 16 compounds under study.

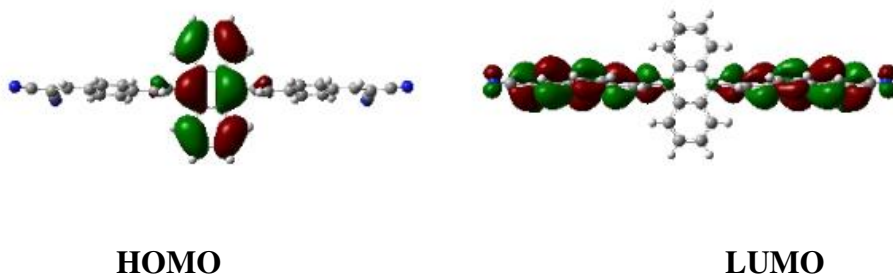


Figure 5. HOMO and LUMO scheme of one of the structure obtained at B3LYP/6-311++G(d,p) level.

The rigid, planar anthracene molecule (A) features a fully conjugated core ring, two enes on either side, and cyano groups, resulting in HOMO and LUMO orbitals distributed across the structure. To effectively separate these frontier molecular orbitals, substituents (R) were introduced to hinder their

free rotation (Figure 4). Geometry-optimized structures of compounds 1–16 are presented in Figures 4 and 5. Although excessive conjugation in planar structures initially hindered orbital separation, tilted geometries with significant dihedral angles successfully achieved a clear distinction between HOMO and LUMO.

Adjusting substituents altered the HOMO and LUMO energy levels, enhancing the compounds' semiconducting properties. Recent studies, such as those on oligomeric thiophene systems for OLED applications (Sengoku et al., 2012), inspired efforts to modify substituents in high-conjugation systems. These modifications aimed to separate HOMO-LUMO distributions and reduce the interfrontier molecular orbital energy gap through conjugation extension. While the geometry-optimized structures did not yield significantly more tilted configurations, the expanded systems led to a narrower HOMO-LUMO energy gap due to increased HOMO energy (Figures 4 and 5).

Compounds 2 and 3, featuring donor-acceptor dihedral angles of 71° for anthracene and 38° for pyrene, demonstrated excellent potential for separating HOMO and LUMO distributions. Across all compounds (1–16), HOMOs localized on donor regions and LUMOs on acceptor regions, ensuring strong semiconducting properties suitable for OLED device applications.

3.2. TADF Properties

Achieving a narrow singlet-triplet energy gap (ΔE_{ST}) between the S1 and T1 states is a critical design criterion for TADF (Thermally Activated Delayed Fluorescence) molecules. This condition is satisfied only when the molecule's lowest-energy transition exhibits a low singlet-triplet exchange energy (Turro, 1991). Research on innovative TADF emitters primarily focuses on intramolecular donor-acceptor (D-A)-type molecules, such as the one discussed here (Li et al., 2014). To design full-color TADF molecules with their HOMO and LUMO localized on different molecular fragments, selecting suitable donor-acceptor units is essential. Time-Dependent Density Functional Theory (TD-DFT) calculations, performed at the B3LYP/6-311++G(d,p) level, provided insights into the geometric and electronic

structures of compounds 1–16. Table 1 presents the HOMO and LUMO energies for these compounds, as well as the ΔE_{ST} values.

The separation of frontier molecular orbitals significantly influences the narrowing of the ΔE_{ST} . For molecule A, the calculated ΔE_{ST} at the B3LYP/6-311++G(d,p) level was 0.65 eV. Compounds 1–16 have been identified as strong TADF candidates, with ΔE_{ST} values below 0.50 eV considered effective for TADF performance. Notably, compounds 4, 5, 9, and 15 exhibit degenerate T_1 and S_1 levels, fully twisted geometries, and highly separated HOMO-LUMO distributions, making them the most promising TADF emitters. For these compounds, particularly **4**, **5**, **9**, and **15**, the ΔE_{ST} values predicted by TD-DFT are sufficiently small to enable thermal repopulation of the S_1 state via reverse intersystem crossing (R_{ISC}) from T_1 to S_1 . Among these, compound **15** demonstrates the greatest potential due to its highly separated HOMO and LUMO orbitals and the narrowest S_1 - T_1 energy gap.

The lowest-energy excited states for all compounds involve an intramolecular charge transfer (ICT) mechanism characterized by low exchange energy. Although the anthracene-thiophene-cyano derivative (16) features a distinct HOMO-LUMO distribution and a 90° dihedral angle, its ΔE_{ST} of 0.65 eV is relatively high, making it less competitive. In contrast, the anthracene-thiophene-lactone system (15), with a dihedral angle of 90° and a ΔE_{ST} of just 0.02 eV, emerges as the most promising candidate due to its exceptionally narrow ΔE_{ST} .

4. CONCLUSION

Nonlinear optical (NLO) phenomena serve as the foundation for various applications in optical sensing, communication systems, and materials science. These phenomena enable us to manipulate light by altering its color, reshaping it in space and time, and producing some of the shortest events ever achieved by humanity. In contrast to linear optics, where a light wave interacts with a molecule, causing it to vibrate and emit a secondary wave that interferes with the original, NLO materials exhibit unique and advanced optical behaviors.

Pyrazine-based organic systems are particularly significant due to their multifunctional roles, including medicinal applications, chemosensing, and optical material development. As a result, the exploration of compounds with potential NLO activity has garnered growing interest within the scientific community. This study computationally investigates anthracene-based potential NLO molecules (1–16) to understand their electronic and structural properties. Given that NLO materials often exhibit OLED activity, these compounds were also theoretically analyzed to evaluate their semiconducting properties. Additionally, thermally activated delayed fluorescence (TADF) activity was assessed to determine the compounds' potential for enhancing quantum yield through fluorescence, driven by excitation and subsequent emission processes.

In this work, well-known donors, such as anthracene, were paired with commonly used acceptors to design potential TADF emitters. Density Functional Theory (DFT) calculations at various theoretical levels were performed to evaluate the structural and electronic features of the compounds. Among the candidates, compounds 9 and 15 emerged as the most promising TADF emitters due to their well-separated HOMO-LUMO orbitals and favorable ΔEST values. Furthermore, all compounds demonstrated interfrontier molecular orbital energy gaps below 4.0 eV, indicating their potential utility as semiconducting materials.

REFERENCES

- Adachi C, Baldo MA, Thompson ME, Forrest SR. Nearly 100% internal phosphorescence efficiency in an organic light-emitting device. *J. Appl. Phys.* 2001, 90, 5048-5051.
- Aydemir M, Haykır G, Battal A, Jankus V, Sugunan SK, Dias FB, Attar H, Türksoy F, Tavaslı M, Monkman AP. High efficiency OLEDs based on anthracene derivatives: The impact of electron donating and withdrawing group on the performance of OLED. *Organic Electronics* 2016, 30, 149-157.
- Atkins P, Overton T, Rourke J, Weller M, Armstrong F., Shriver & Atkins *Inorganic Chemistry*, Fourth Edition, Oxford University Press, Oxford, 2006.
- Baldo MA, OBrien DA, Thompson ME, Forrest SR. Excitonic singlet-triplet ratio in a semiconducting organic thin film. *Phys. Rev. B* 1999, 60, 14422-14428.
- Baldo MA, OBrien DF, You Y, Shoustikov A, Sibley S, Thompson ME, Forrest SR. Highly efficient phosphorescent emission from organic electroluminescent devices. *Nature* 1998, 395, 151-154.
- Baldo MA, S. Lamansky , P. E. Burrows , Thompson ME, Forrest SR. Very high-efficiency green organic light-emitting devices based on electrophosphorescence. *Appl. Phys. Lett.* 1999, 75, 4-6.
- Becke AD. Density-functional exchange-energy approximation with correct asymptotic behavior. *Phys Rev A* 1988, 38, 3098–3100.
- Binggeli C. *Interior Graphic Standards: Student Edition*. New Jersey, Wiley, 2012.
- Tsai YS, Hong LA, Juang FS, Chen CY. Blue and white phosphorescent organic light emitting diode performance improvement by confining electrons and holes inside double emitting layers. *J Lumin* 2014, 153, 312-316.
- Casida ME, Jamorski C, Casida KC, Salahub DR. Molecular excitation energies to high-lying bound states from time-dependent density-functional response theory: characterization and correction of the time-dependent local density approximation ionization threshold. *J Chem Phys* 1998, 108, 4439–4449.

- Czerwieńiec R, Yu J, Yersin H. Blue-Light Emission of Cu(I) Complexes and Singlet Harvesting. *Inorg Chem* 2011, 50, 8293-8301.
- Çiçek B, Çalışır Ü, Tavaslı M, Tülek R, Teke A. Synthesis and optical characterization of novel carbazole Schiff bases. *J Mol Struct* 2018, 1153, 42-47.
- deSa GF, Malta OL, deMello DC, Simas AM, Longo RL, Santa-Cruz PA, daSilva EF. Spectroscopic properties and design of highly luminescent lanthanide coordination complexes. *Coord Chem Rev* 2000, 196, 165–195.
- Endo A, Ogasawara M, Takahashi A, Yokoyama D, Kato Y, Adachi C. Thermally Activated Delayed Fluorescence from Sn⁴⁺-Porphyrin Complexes and Their Application to Organic Light Emitting Diodes — A Novel Mechanism for Electroluminescence. *Adv Mater* 2009, 21, 4802-4806.
- Endo A, Sato K, Yoshimura K, Kai T, Kawada A, Miyazaki H, Adachi C. Efficient up-conversion of triplet excitons into a singlet state and its application for organic light emitting diodes. *Appl Phys Lett* 2011, 98, 083302-083302.
- Frisch, M. J., Trucks, G. W., Schlegel, H. B., Scuseria, G. E., Robb, M. A., Cheeseman, J. R., Scalmani, G., Barone, V., Petersson, G. A., Nakatsuji, H., Li, X., Caricato, M., Marenich, A. V., Bloino, J., Janesko, B. G., Gomperts, R., Mennucci, B., Hratchian, H. P., Ortiz, J. V., Izmaylov, A. F., Sonnenberg, J. L., Williams-Young, D., Ding, F., Lipparini, F., Egidi, F., Goings, J., Peng, B., Petrone, A., Henderson, T., Ranasinghe, D., Zakrzewski, V. G., Gao, J., Rega, N., Zheng, G., Liang, W., Hada, M., Ehara, M., Toyota, K., Fukuda, R., Hasegawa, J., Ishida, M., Nakajima, T., Honda, Y., Kitao, O., Nakai, H., Vreven, T., Throssell, K., Montgomery, Jr., J. A., Peralta, J. E., Ogliaro, F., Bearpark, M. J., Heyd, J. J., Brothers, E. N., Kudin, K. N., Staroverov, V. N., Keith, T. A., Kobayashi, R., Normand, J., Raghavachari, K., Rendell, A. P., Burant, J. C., Iyengar, S. S., Tomasi, J., Cossi, M., Millam, J. M., Klene, M., Adamo, C., Cammi, R., Ochterski, J. W., Martin, R. L., Morokuma, K., Farkas, O., Foresman, J. B., & Fox, D.J. (2016) Gaussian, Inc., Wallingford CT.

- Fourassier C. Luminescence Encyclopedia of Inorganic Chemistry. New York, Academic Press, 1984.
- Ivanov MA, Puzyk MV, Balashev KP. Spectroscopic and Electrochemical Properties of Dichlorodiimine Complexes of Au(III) and Pt(II) with 1,4-Diazine Derivatives of o-Phenanthroline. *Russ J Gen Chem* 2006, 76, 843-848.
- Kalyani NT, Swart H, Dhoble SJ. Principles and Applications of Organic Light Emitting Diodes (OLEDs). Duxford, United Kingdom, Woodhead Printing, 2017.
- Kohn W, Sham LJ. Self-consistent equations including exchange and correlation effects. *Phys. Rev.* 1965, 140, 1133-1138.
- Karton A, Tarnopolsky A, Lamre JF, Schatz GC, Martin JML. Highly Accurate First-Principles Benchmark Data Sets for the Parametrization and Validation of Density Functional and Other Approximate Methods. Derivation of a Robust, Generally Applicable, Double-Hybrid Functional for Thermochemistry and Thermochemical Kinetics. *J. Phys. Chem. A*, 2008, 112 (50), pp 12868–12886.
- Khodae Z, Yahyazadeh A, Mahmoodi NO, Zanjanchi MA, Azimi V. One-pot synthesis and characterization of new cuprous pyrazinoporphyrazines containing peripherally functionalized units. *J Mol Struct* 2012, 1029, 92–97.
- Lee C, Yang W, Parr RG, Development of the Colle–Salvetti correlation energy formula into a functional of the electron density. *Phys Rev B* 1988, 37, 785–789.
- Leitl MJ, Küchle FR, Mayer HA, Wesemann L, Yersin H. Brightly Blue and Green Emitting Cu(I) Dimers for Singlet Harvesting in OLEDs. *J. Phys Chem A* 2013, 117, 11823-11836.
- Li P, Cui Y, Song C, Zhang H. A systematic study of phenoxazine-based organic sensitizers for solar cells. *Dyes and Pigments* 2017, 137, 12-23.
- Li J, Zhang Q, Nomura H, Miyazaki H, Adachi C. Thermally Activated Delayed Fluorescence from $n\pi^*$ to $\pi\pi^*$ up-Conversion and its Application to Organic Light- Emitting Diodes, *Appl Phys Lett* 2014, 105, 013301-013304.

- Lindsey, Jonathan; et al. "Anthracene". PhotochemCAD. Retrieved 20 February 2014.
- Liu YF, Feng J, Zhang YF, Cui HF, Yin D, Bi YG, Song JF, Chen QD, Sun HB. Improved efficiency of indium-tin-oxide-free flexible organic light-emitting devices. *Org Electron* 2014, 15, 478–483.
- Mc Keever SW. *Thermoluminescence in Solids*. Cambridge, Cambridge University Press, 1985.
- Meerholz K, Müller DC. Outsmarting Waveguide Losses in Thin-Film Light-Emitting Diodes. *Adv. Funct. Mater.* 2001, 11, 251-253.
- Mehes G, Nomura H, Zhang Q, Nakagawa T, Adachi C. Enhanced electroluminescence efficiency in a spiro-acridine derivative through thermally activated delayed fluorescence. *Angew Chem Int Ed* 2012, 51, 11311-11315.
- Nakagawa T, Ku SY, Wong KT, Adachi C. Electroluminescence based on thermally activated delayed fluorescence generated by a spirobifluorene donor–acceptor structure. *Chem Commun* 2012, 48, 9580-9582.
- Nasu K, Nakagawa T, Nomura H, Lin CJ, Cheng CH, Tseng MR, Yasuda T, Adachi C. A highly luminescent spiro-anthracenone-based organic light-emitting diode exhibiting thermally activated delayed fluorescence, *Chem Commun* 2013, 49, 10385-10387.
- Nishida JI, Murai S, Fujiwara E, Tada H, Tomura M, Yamashita Y. Preparation, Characterization, and FET Properties of Novel Dicyanopyrazinoquinoxaline Derivatives. *Org Lett* 2004, 6, 2007-2010.
- OBrien DF, Baldo MA, Thompson ME, Forrest SR. Improved energy transfer in electrophosphorescent devices. *Appl. Phys. Lett.* 1999, 74, 442-444.
- Patel BN, Prajapati MM. *OLED: A Modern Display Technology*. Interof Sci Res Pub 2014, 4, 1-5.
- Schlyer BD, Schauerte JA, Steel DG, Gafni A. Time-resolved room temperature protein phosphorescence: nonexponential decay from single emitting tryptophans. *Biophys J* 1994, 67, 1192-202.

- Segal M, Baldo MA, Holmes RJ, Forrest SR, Soos ZG. Excitonic singlet-triplet ratios in molecular and polymeric organic materials. *Phys Rev B* 2003, 68, 075211-075226.
- Seo JA, Gong MS, Song W, Lee JY. Molecular Orbital Controlling Donor Moiety for High-Efficiency Thermally Activated Delayed Fluorescent Emitters. *Chem. Asian J.* 2016, 11, 868 – 873.
- Sengoku T, Yamao T, Hotta S. Organic light-emitting diodes based on layered films of thiophene/phenylene co-oligomers. *J Non-Crystalline Solids* 2012, 358, 2525–2529.
- Shan T, Gao Z, Tang X, He X, Gao Y, Li J, Sun X, Liu Y, Liu H, Yang B, Lu P, Ma Y. Highly efficient and stable pure blue nondoped organic light-emitting diodes at high luminance based on phenanthroimidazole-pyrene derivative enabled by triple-triplet annihilation. *Dyes and Pigments* 2017, 142, 189-197.
- Sparks JS, Schelly RC, Smith WL, Davis MP, Tchernov D, Pierivone VA, Gruber DF. The Covert World of Fish Biofluorescence: A Phylogenetically Widespread and Phenotypically Variable Phenomenon. *PLoS One* 2014, 9, e83259.
- Sun Y, Giebink NC, Kanno H, Ma B, Thompson ME, Forrest SR. Excitonic singlet-triplet ratio in a semiconducting organic thin film. *Phys. Rev. B* 1999, 60, 14422-14428.
- Turro NJ. *Modern Molecular Photochemistry*, University Science Books, 1991.
- Uoyama H, Goushi K, Shizu K, Nomura H, Adachi C. Highly efficient organic light-emitting diodes from delayed fluorescence. *Nature* 2012, 492, 234-238.
- Wang S, Yan X, Cheng Z, Zhang H, Liu Y, Wang Y. Highly Efficient Near-Infrared Delayed Fluorescence Organic Light Emitting Diodes Using a Phenanthrene-Based Charge-Transfer Compound. *Angew Chem Int Ed* 2015, 54, 13068–13072.
- Wilson JS, Dhoot AS, Seeley AJAB, Khan MS, Köhler A, Friend RH. Spin-dependent exciton formation in π -conjugated compounds. Spin-dependent exciton formation in π -conjugated compounds. *Nature* 2001, 413, 828-431.

- Xiaoxiao W, Fushan L, Wei W, Tailiang G. Flexible white phosphorescent organic light emitting diodes based on multilayered graphene/PEDOT:PSS transparent conducting film. *Appl Surf Sci* 2014, 295, 214–218.
- Yanez SM, Moya SA, Zuniga C, Jiron GC. Theoretical assessment of TD-DFT applied to a ferrocene-based complex. *Comput Theor Chem* 2017, 1118, 65–74.
- Zhang QY, Pita K, Buddhudu S, Kam CH. *J Phys D* 2002, 35, 3085–3090.
- Zhao Y, Truhlar DG. The M06 suite of density functionals for main group thermochemistry, thermochemical kinetics, noncovalent interactions, excited states, and transition elements: two new functionals and systematic testing of four M06-class functionals and 12 other functionals. *Theor Chem Acc* 2008, 120, 215-241.
- Zhao Y, Truhlar DG. Density Functional for Spectroscopy: No Long-Range Self-Interaction Error, Good Performance for Rydberg and Charge-Transfer States, and Better Performance on Average than B3LYP for Ground States. *J Phys Chem A* 2006, 110, 13126-13130.
- Zhao Y, Truhlar DG. A new local density functional for main-group thermochemistry, transition metal bonding, thermochemical kinetics, and noncovalent interactions. *J Chem Phys* 2006, 125, 194101-194118.



ISBN: 978-625-378-052-4